Impedance-Based Fault Location in Transmission Networks: Theory and Application

SWAGATA DAS[1], (Student Member, IEEE), SURYA SANTOSO[1], (Senior Member, IEEE), ANISH GAIKWAD[2], (Member, IEEE), AND MAHENDRA PATEL[2], (Senior Member, IEEE)

[1]Department of Electrical and Computer Engineering, The University of Texas at Austin, Austin, TX 78712, USA
[2]Electric Power Research Institute, Knoxville, TN 37932, USA

Corresponding author: S. Santoso (ssantoso@mail.utexas.edu)

ABSTRACT A number of impedance-based fault location algorithms have been developed for estimating the distance to faults in a transmission network. Each algorithm has specific input data requirements and makes certain assumptions that may or may not hold true in a particular fault location scenario. Without a detailed understanding of the principle of each fault-locating method, choosing the most suitable fault location algorithm can be a challenging task. This paper, therefore, presents the theory of one-ended (simple reactance, Takagi, modified Takagi, Eriksson, and Novosel *et al.*) and two-ended (synchronized, unsynchronized, and current-only) impedance-based fault location algorithms and demonstrates their application in locating real-world faults. The theory details the formulation and input data requirement of each fault-locating algorithm and evaluates the sensitivity of each to the following error sources: 1) load; 2) remote infeed; 3) fault resistance; 4) mutual coupling; 5) inaccurate line impedances; 6) DC offset and CT saturation; 7) three-terminal lines; and 8) tapped radial lines. From the theoretical analysis and field data testing, the following criteria are recommended for choosing the most suitable fault-locating algorithm: 1) data availability and 2) fault location application scenario. Another objective of this paper is to assess what additional information can be gleaned from waveforms recorded by intelligent electronic devices (IEDs) during a fault. Actual fault event data captured in utility networks is exploited to gain valuable feedback about the transmission network upstream from the IED device, and estimate the value of fault resistance.

INDEX TERMS Fault location, impedance-measurement, intelligent electronic devices (IED), power system faults, power system reliability, transmission line measurements.

NOMENCLATURE

ρ	Earth resistivity ($\Omega\,m$)
d_s	Current distribution factor
β	Phase angle of d_s (degrees)
m	Distance to the fault (pu)
D	Distance of the tap point from terminal G (pu)
R_F	Fault resistance (Ω)
I_F	Current at the fault point F (kA)
I_T	Fault current from terminal T (kA)
I_{J0}	Zero-sequence current in the parallel transmission line at terminal G (kA)
V_{Tap}	Voltage at the tap point during the fault (kV)
Z_{app}	Apparent impedance to the fault (Ω)
Z_{0M}	Zero-sequence mutual coupling (Ω)
Z_{012}	Sequence line impedance matrix (Ω)
Z_{Load}	Load impedance (Ω)
V_{F1pre}	Positive-sequence prefault voltage at the fault point F (kV)
V_{AB}, V_{CA}	Line-to-line fault voltages between phases A and B, and phases C and A (kV)
E_G, E_H	Internal source voltages at terminals G and H (kV)
Z_G, Z_H	Source impedances behind terminals G and H (Ω)
I_G, I_H	Line currents during the fault at terminals G and H (kA)
V_G, V_H	Line-to-ground voltages recorded during the fault at terminals G and H (kV)
I_J, I_K	Line currents in the parallel transmission line at terminals G and H (kA)
I_{J2}, I_{K2}	Negative-sequence currents in the parallel transmission line at terminals G and H (kA)

$\Delta V_G, \Delta V_H$	"Pure fault" voltages at terminals G and H (kV)
$\Delta I_G, \Delta I_H$	"Pure fault" currents at terminals G and H (kA)
$I_{Apre}, I_{Bpre}, I_{Cpre}$	Prefault currents in phases A, B, and C at terminal G (kA)
V_{G1pre}, V_{H1pre}	Positive-sequence prefault voltages at terminals G and H (kV)
I_{G1pre}, I_{H1pre}	Positive-sequence prefault currents at terminals G and H (kA)
I_{G0}, I_{G1}, I_{G2}	Sequence components of the fault current at terminal G (kA)
I_{H0}, I_{H1}, I_{H2}	Sequence components of the fault current at terminal H (kA)
I_{AF}, I_{BF}, I_{CF}	Fault currents in phases A, B, and C at terminal G (kA)
V_{AF}, V_{BF}, V_{CF}	Fault voltages in phases A, B, and C at terminal G (kV)
V_{G0}, V_{G1}, V_{G2}	Sequence components of the fault voltage at terminal G (kV)
V_{H0}, V_{H1}, V_{H2}	Sequence components of the fault voltage at terminal H (kV)
V_{F0}, V_{F1}, V_{F2}	Sequence components of the voltage at the fault point F (kV)
Z_{L0}, Z_{L1}, Z_{L2}	Sequence components of the line impedance between terminals G and H (Ω)
Z_{G0}, Z_{G1}, Z_{G2}	Sequence components of the Thevenin impedance behind terminal G (Ω)
Z_{H0}, Z_{H1}, Z_{H2}	Sequence components of the Thevenin impedance behind terminal H (Ω)

I. INTRODUCTION

Transmission lines are often subjected to electrical faults due to lightning strikes during stormy weather conditions, animal or tree contact with a transmission line, or insulation failure in power system equipment. To expedite service restoration and improve system reliability, impedance-based fault location algorithms are commonly used to determine the location of transmission line faults since they are straightforward to implement and yield reasonable location estimates [1], [2]. Voltage and current waveforms captured during a fault by intelligent electronic devices (IEDs) such as digital relays, digital fault recorders, and sequence event recorders are used to estimate the apparent impedance between the IED device and the location of the short-circuit fault. Given the line impedance in ohms, the per-unit distance to the fault can be estimated accurately.

A number of impedance-based fault location algorithms have been developed for transmission network applications. Fault-locating algorithms using data captured by an IED device at one end of the line are commonly referred to as one-ended algorithms, while those using data captured by IEDs at both ends of a transmission line are referred to as two-ended algorithms. Each algorithm has specific input data requirements and makes certain assumptions when

computing the distance to a fault. These assumptions may or may not hold true in a particular fault location scenario. Put another way, no single fault-locating algorithm works best in several different fault location scenarios. Choosing the best approach for locating faults from such a wide selection of impedance-based fault location algorithms is, therefore, an overwhelming task and requires a detailed understanding of the working principle behind each fault-locating algorithm.

Based on the aforementioned background, this paper presents the underlying theory of one-ended impedance-based fault location algorithms (simple reactance, Takagi, modified Takagi, Eriksson, and Novosel *et al.* methods) and two-ended impedance-based fault location algorithms (synchronized, unsynchronized, and current-only methods). The objectives are to clearly define the input data requirement of each fault-locating algorithm, quantify the various sources of fault-locating error, demonstrate the application of each algorithm in locating real-world transmission line faults, and provide recommendations for choosing the best fault-locating approach. Fault-locating error sources evaluated include load, fault resistance, remote infeed, mutual coupling in parallel lines, DC offset and CT saturation, inaccurate line impedances as well as challenging application scenarios such as three-terminal and tapped radial lines. A similar objective explored by the authors in [3]–[6] pertains to distribution networks only. Although the fault-locating principle remains the same, many of the fault location algorithms and error sources are different and specific only to transmission networks, which is the focus of this paper. Authors in [7]–[9] investigate the impact of various fault-locating error sources on a limited number of algorithms. References [10] and [11] are excellent resources for impedance-based fault location algorithms. Unfortunately, the discussion in [10] is limited to one-ended methods, while [11] does not encompass all the impedance-based fault location algorithms described in the IEEE C37.114 Standard [1].

In addition to computing the location of a fault, event reports recorded by intelligent electronic devices (IEDs) capture the response of the power system to a disturbance such as a fault and contain a wealth of information. Therefore, another objective of this paper is to assess what additional information can be gleaned from IED data. Using field event data captured in utility circuits, this paper demonstrates how IED data can be used to estimate the value of fault resistance. Interpretation of this value is useful for identifying the root-cause of the fault [12] and also for validating the short-circuit model of the transmission network. Moreover, fault event data can be used to gain valuable feedback about the state of the transmission network upstream from the IED location.

The paper is organized as follows. Section II describes the principle of impedance-based fault location algorithms in detail and also defines the input data required for performing fault location. Section III evaluates the sensitivity of fault location algorithms to various sources of fault-locating error. A simple test case is used to evaluate the performance of each fault-locating method, given a particular error source.

Section IV demonstrates the application of impedance-based fault location algorithms to actual fault event data collected from utility networks. Each event highlights a unique aspect of impedance-based fault location and also illustrates the potential benefits of IED data. Finally, Section V summarizes the lessons learned from the analysis in this paper and recommends the following criteria for selecting the best approach for fault location: (a) data availability, and (b) fault location application scenario.

II. THEORY OF IMPEDANCE-BASED FAULT LOCATION ALGORITHMS

This Section reviews the one- and two-ended impedance-based fault location algorithms that are commonly used to locate faults in a transmission network. The goals are to define the input data requirement of each method and identify the different factors that affect the accuracy of location estimates.
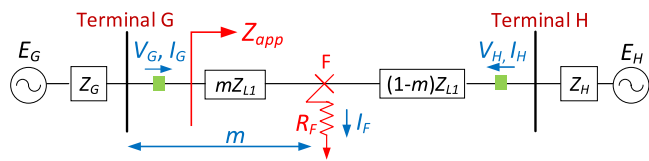
FIGURE 1. One-line Diagram of a Two-terminal Transmission Network.

A. ONE-ENDED IMPEDANCE-BASED FAULT LOCATION ALGORITHMS

As the name suggests, one-ended impedance-based fault location algorithms estimate the location of a fault by looking into a transmission line from one end [1] as illustrated in Fig. 1. Voltage and current waveforms captured during a fault by an intelligent electronic device (IED) at one end of the line are used to determine the apparent impedance between the IED device and the location of the short-circuit fault. Given the impedance of the transmission line in ohms, the per-unit distance to a fault can be easily obtained. The advantages of using one-ended algorithms are that they are straightforward to implement, yield reasonable location estimates, and require data from only one end of a line. There is no need for any communication channel or remote data and hence, fault location can be implemented at the line terminal by any microprocessor-based numerical relay.

To illustrate the principle of one-ended methods, consider the two-terminal transmission network shown in Fig. 1. The transmission line is homogeneous and has a total positive-sequence impedance of Z_{L1} between terminals G and H. Networks upstream from terminals G and H are represented by their respective Thevenin equivalents having impedances Z_G and Z_H. When a fault with resistance R_F occurs at a distance m per unit from terminal G, both sources contribute to the total fault current I_F. The voltage and current phasors recorded at terminal G during the fault are V_G and I_G, respectively. Similarly, the voltage and current phasors recorded at terminal H during the fault are V_H and I_H, respectively. It should be noted that although measurements are available

TABLE 1. Definition of V_G, I_G, and ΔI_G for different fault types.

Fault Type	V_G	I_G	ΔI_G
A-G	V_{AF}	$I_{AF} + kI_{G0}$	$I_{AF} - I_{Apre}$
B-G	V_{BF}	$I_{BF} + kI_{G0}$	$I_{BF} - I_{Bpre}$
C-G	V_{CF}	$I_{CF} + kI_{G0}$	$I_{CF} - I_{Cpre}$
AB, AB-G, ABC	$V_{AF} - V_{BF}$	$I_{AF} - I_{BF}$	$\begin{pmatrix} I_{AF} - I_{Apre} \end{pmatrix} - \begin{pmatrix} I_{BF} - I_{Bpre} \end{pmatrix}$
BC, BC-G, ABC	$V_{BF} - V_{CF}$	$I_{BF} - I_{CF}$	$\begin{pmatrix} I_{BF} - I_{Bpre} \end{pmatrix} - \begin{pmatrix} I_{CF} - I_{Cpre} \end{pmatrix}$
CA, CA-G, ABC	$V_{CF} - V_{AF}$	$I_{CF} - I_{AF}$	$\begin{pmatrix} I_{CF} - I_{Cpre} \end{pmatrix} - \begin{pmatrix} I_{AF} - I_{Apre} \end{pmatrix}$

where $k = \dfrac{Z_{L0}}{Z_{L1}} - 1$

at both ends of the line, one-ended methods use the voltage and current captured at terminal G or at terminal H. Using Kirchhoff's laws, the voltage drop from terminal G can be expressed as

$$V_G = mZ_{L1}I_G + R_F I_F \quad (1)$$

where the form taken by V_G and I_G depends on the fault type and are defined in Table 1. Dividing throughout by I_G, the apparent impedance to the fault (Z_{app}) measured from terminal G can be expressed as

$$Z_{app} = \frac{V_G}{I_G} = mZ_{L1} + R_F \left(\frac{I_F}{I_G} \right) \quad (2)$$

Equation 2 is the fundamental equation that governs one-ended impedance-based fault location algorithms. Unfortunately, because measurements from only one end of the line are used, (2) has three unknowns, namely, m, R_F, and I_F. In order to eliminate R_F and I_F from the fault location computation, several one-ended algorithms have been developed and are discussed in details below.
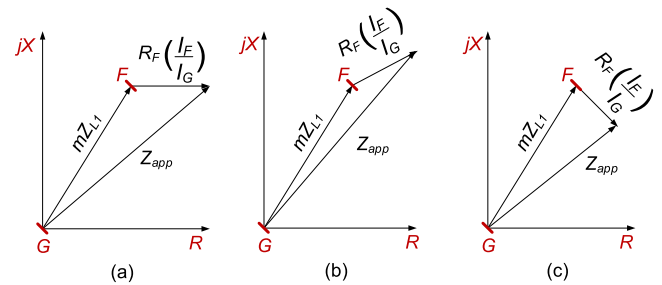
FIGURE 2. Reactance Error in the Simple Reactance Method [13] .
(a) $\angle I_F = \angle I_G$. (b) $R_F \neq 0\ \Omega$, I_F leads I_G. (c) $R_F \neq 0\ \Omega$, I_F lags I_G.

1) SIMPLE REACTANCE METHOD

The simple reactance method takes advantage of the fact that fault resistance R_F is resistive in nature. Therefore, if currents I_F and I_G are assumed to be in phase, the term $R_F (I_F/I_G)$ in (2) reduces to a real number as illustrated in Fig. 2(a). Considering only the imaginary components of (2), the distance

to a fault is given by

$$m = \frac{\text{imag}\left(\frac{V_G}{I_G}\right)}{\text{imag}\left(Z_{L1}\right)} \qquad (3)$$

Put another way, the simple reactance method estimates the reactance to a fault in order to eliminate R_F from the fault location calculation. The method is computationally simple and requires minimum data for fault location. However, the accuracy of the distance to fault estimates is severely affected when I_F and I_G are not in phase. The phase angle mismatch can be attributed to the system load present at the time of the fault. Furthermore, in a non-homogeneous system, currents I_H and I_G do not have the same phase angle. Because I_F is the summation of I_G and I_H, the phase angle of I_F is also not equal to that of I_G. As a result, R_F (I_F/I_G) is a complex number and presents an additional reactance to the fault. Neglecting this reactance introduces an error in the location estimates and is referred to as the reactance error [1]. When I_F leads I_G, the term R_F (I_F/I_G) is inductive and increases the apparent impedance to the fault as shown in Fig. 2(b). One-ended methods will, therefore, overestimate the location of the fault. When I_F lags I_G, the term R_F (I_F/I_G) is capacitive and decreases the apparent impedance to the fault as shown in Fig. 2 (c). In such cases, one-ended methods will underestimate the location of the fault.
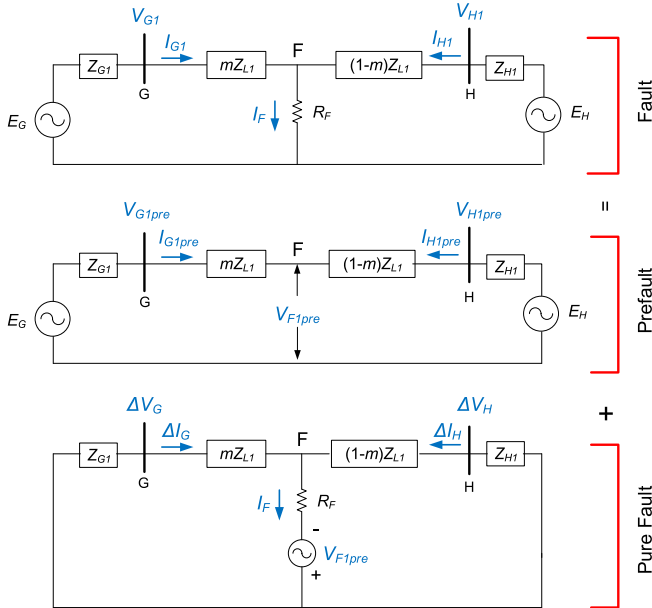

FIGURE 3. Superposition Theorem used to Decompose the Network in Fig. 1 during a Three-phase Fault.

2) TAKAGI METHOD

The Takagi method improves upon the performance of the simple reactance method by "subtracting out" [2] the load current from the total fault current. Using the superposition principle, the network during a fault is decomposed into a prefault and "pure fault" network as illustrated in Fig. 3

for a three-phase fault. In a "pure fault" network, all voltage sources are short-circuited and a voltage source, V_{F1pre}, is inserted at the fault point F. Applying the current division rule to the "pure fault" network, the fault current I_F is calculated as [14]

$$I_F = \left(\frac{Z_{G1} + Z_{L1} + Z_{H1}}{(1-m)Z_{L1} + Z_{H1}}\right)\Delta I_G = \frac{1}{|d_s| \angle \beta} \times \Delta I_G \quad (4)$$

where d_s is the current distribution factor and β is the angle of the current distribution factor. Substituting the expression for I_F in (1) and multiplying both sides by the complex conjugate of ΔI_G, the following is obtained:

$$V_G \times \Delta I_G^* = mZ_{L1}I_G\Delta I_G^* + R_F \times \left(\frac{1}{d_s}\right) \qquad (5)$$

To eliminate R_F from the fault location computation in (5), Takagi method assumes that the transmission network is homogeneous, i.e., the local and remote source impedances, Z_G and Z_H, have the same impedance angle as the transmission line. This assumption implies that d_s is a real number with β equal to zero. As a result, the term $R_F(1/d_S)$ reduces to a real number. Equating only the imaginary components of (5), the distance to a fault is given as

$$m = \frac{\text{imag}\left(V_G \times \Delta I_G^*\right)}{\text{imag}\left(Z_{L1} \times I_G \times \Delta I_G^*\right)} \qquad (6)$$

where V_G, I_G, and ΔI_G depend on the fault type and are defined in Table 1.

Although the Takagi method uses the "pure fault" current ΔI_G to minimize any reactance error caused by the system load, the success of this method relies on the transmission network being homogeneous in nature. If the system is non-homogeneous, $R_F(1/d_S)$ is no longer a real number and will cause a reactance error in the location estimates. The error is proportional to the degree of non-homogeneity. In addition, when calculating ΔI_G, the method assumes that the load current remains equal both before and during the fault. This holds true for a constant current load model only. In practice, loads are a mix of constant power and constant impedance loads with very few loads being constant current in nature.

3) MODIFIED TAKAGI METHOD

Depending on relay settings, the prefault current may not be available for fault location purposes. To avoid using the prefault current, the modified Takagi method uses the zero-sequence current I_{G0} instead of ΔI_G to account for the system load during a single line-to-ground fault [7], [11]. This simple substitution is possible due to the fact that I_{G0}, similar to ΔI_G, exists only during a ground fault and is zero under balanced operating conditions. Distance to a fault is computed from the following expression:

$$m = \frac{\text{imag}\left(V_G \times 3I_{G0}^*\right)}{\text{imag}\left(Z_{L1} \times I_G \times 3I_{G0}^*\right)} \qquad (7)$$

In addition, to compensate for a non-homogeneous system, the modified Takagi method uses the zero-sequence network
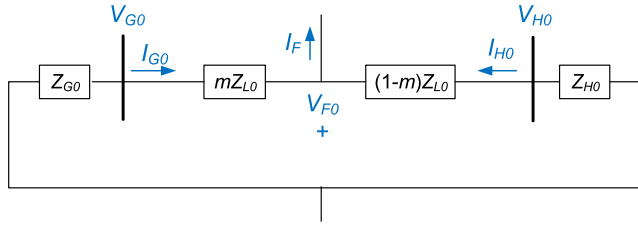
FIGURE 4. Zero-sequence Network during a Ground Fault.

shown in Fig. 4 to calculate d_s as

$$|d_s| \angle \beta = \frac{Z_{G0} + Z_{L0} + Z_{H0}}{(1-m)Z_{L0} + Z_{H0}} \qquad (8)$$

Since β represents the degree of non-homogeneity, applying an angle correction of $e^{-j\beta}$ to the fault location computation in (7) would force the system to be homogeneous and improve the accuracy of location estimates. However, to calculate β, the distance to fault m must be known. Therefore, the modified Takagi method proceeds by first calculating a preliminary estimate of m using (7). This value of m is then used to calculate the angle correction factor in (8). The final fault location estimate that accounts for both load and system non-homogeneity is

$$m = \frac{\text{imag}\left(V_G \times 3I_{G0}^* \times e^{-j\beta}\right)}{\text{imag}\left(Z_{L1} \times I_G \times 3I_{G0}^* \times e^{-j\beta}\right)} \qquad (9)$$

Although the modified Takagi method has a superior performance over the Takagi method, the accuracy of location estimates depends on accurately knowing the source impedance parameters. If the zero-sequence impedance of the local source is not available, it may be estimated from the fault data as

$$Z_{G0} = -\frac{V_{G0}}{I_{G0}} \qquad (10)$$

The remote source impedance, Z_{H0}, however, must be known.

4) ERIKSSON METHOD
To compute the distance to a fault, this method uses the source impedance parameters to overcome any reactance error caused by fault resistance, load, or system non-homogeneity [15]. Moreover, this method also estimates the value of fault resistance, which is useful for identifying the root-cause of a fault and for validating the short-circuit model of a transmission network [16]. The current distribution factor d_s is directly substituted in (5) as

$$V_G = mZ_{L1}I_G + R_F \left(\frac{Z_{G1} + Z_{L1} + Z_{H1}}{(1-m)Z_{L1} + Z_{H1}}\right)\Delta I_G \qquad (11)$$

Simplifying and rearranging the terms results in the following expression:

$$m^2 - k_1 m + k_2 - k_3 R_F = 0 \qquad (12)$$

where constants k_1, k_2, and k_3 are complex multiplications of voltage, current, line impedance, and source impedances and

are defined as follows:

$$k_1 = a + jb = 1 + \frac{Z_{H1}}{Z_{L1}} + \left(\frac{V_G}{Z_{L1} \times I_G}\right)$$

$$k_2 = c + jd = \frac{V_G}{Z_{L1} \times I_G}\left(1 + \frac{Z_{H1}}{Z_{L1}}\right)$$

$$k_3 = e + jf = \frac{\Delta I_G}{Z_{L1} \times I_G}\left(1 + \frac{Z_{H1} + Z_{G1}}{Z_{L1}}\right)$$

Separating (12) into real and imaginary parts, the distance to fault m can be solved from the following quadratic equation:

$$m = \frac{\left(a - \frac{eb}{f}\right) \pm \sqrt{\left(a - \frac{eb}{f}\right)^2 - 4\left(c - \frac{ed}{f}\right)}}{2} \qquad (13)$$

where m can take two possible values. Since the fault location estimate must be less that the total line length, the value of m that lies between 0 and 1 per unit should be chosen as the location estimate. Fault resistance can then be calculated as

$$R_F = \frac{d - mb}{f} \qquad (14)$$

If the local source impedance Z_{G1} is not available, it can be calculated from the fault event data as

$$Z_{G1} = -\frac{V_{G1} - V_{G1pre}}{I_{G1} - I_{G1pre}} \qquad (15)$$

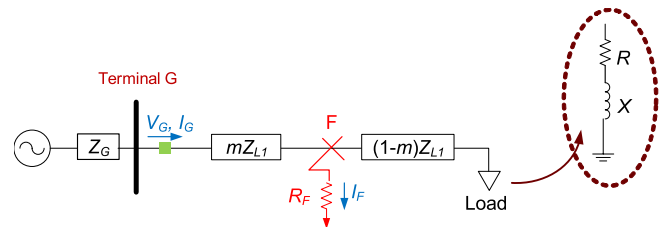The remote source impedance Z_{H1} must be accurately known.

FIGURE 5. Novosel et al. Method is Applicable to a Radial Transmission Line Only. Load Model is assumed to be Constant Impedance in Nature.

5) NOVOSEL et al. METHOD
This fault-locating technique is a modified version of the Eriksson method and is applicable for locating faults on a short, radial transmission line [17]. All loads served by the transmission line are lumped at the end of the feeder as shown in Fig. 5. Assuming a constant impedance load model, the first step consists of estimating the load impedance from the prefault voltage and current as

$$Z_{Load} = R + jX = \frac{V_{G1pre}}{I_{G1pre}} - Z_{L1} \qquad (16)$$

The per-unit distance to the fault can be obtained by solving the quadratic equation in (13), where the constants are

defined as

$$k_1 = a + jb = 1 + \frac{Z_{Load}}{Z_{L1}} + \left(\frac{V_G}{Z_{L1} \times I_G}\right)$$

$$k_2 = c + jd = \frac{V_G}{Z_{L1} \times I_G}\left(1 + \frac{Z_{Load}}{Z_{L1}}\right)$$

$$k_3 = e + jf = \frac{\Delta I_G}{Z_{L1} \times I_G}\left(1 + \frac{Z_{Load} + Z_{G1}}{Z_{L1}}\right)$$

The value of m which lies between 0 and 1 per unit is chosen as the location estimate. If the local source impedance Z_{G1} is not known, it can be estimated from (15). Similar to the Eriksson method, the Novosel *et al.* method is also robust to any reactance error due to fault resistance and load. Additional benefits include estimating the fault resistance from the expression in (14).

B. TWO-ENDED IMPEDANCE-BASED FAULT LOCATION ALGORITHMS

Two-ended impedance-based algorithms use waveform data captured at both ends of a transmission line to estimate the location of a fault. The fault-locating principle is similar to that of one-ended methods, i.e., using the voltage and current during a fault to estimate the apparent impedance from the monitoring location to the fault. Additional measurements from the remote end of a transmission line are used to eliminate any reactance error caused by fault resistance, load current, or system non-homogeneity. Fault type classification is also not required. A communication channel transfers the data from one IED device to the other. Alternatively, data from both IEDs can be collected and processed at a central location. Depending on data availability, two-ended impedance-based methods are further classified as follows:
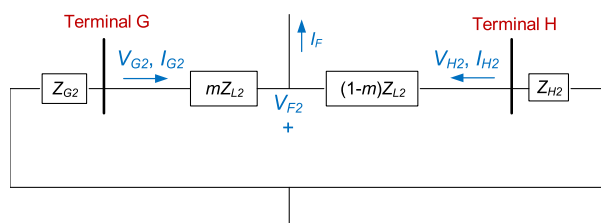

FIGURE 6. Negative-sequence Network during an Unbalanced Fault.

1) SYNCHRONIZED TWO-ENDED METHOD

This method assumes that measurements from both ends of a transmission line are synchronized to a common time reference via a global positioning system (GPS). Any one of the three symmetrical components can be used for fault location computation. Using the negative-sequence components are, however, more advantageous since they are not affected by load current, zero-sequence mutual coupling, uncertainty in zero-sequence line impedance, or infeed from zero-sequence tapped loads [10], [18]. To illustrate the fault-locating principle, consider the negative-sequence network during an unbalanced fault as shown in Fig. 6. V_{F2} is the negative-sequence voltage at the fault point F and can be

calculated from terminal G and H as

Terminal G: $\quad V_{F2} = V_{G2} - mZ_{L2}I_{G2}$ \hfill (17)

Terminal H: $\quad V_{F2} = V_{H2} - (1-m)Z_{L2}I_{H2}$ \hfill (18)

Voltage V_{F2} is equal when calculated from either line terminal. Therefore, equating (17) and (18), the distance to fault (m) can be computed as

$$m = \frac{V_{G2} - V_{H2} + Z_{L2}I_{H2}}{(I_{G2} + I_{H2})\,Z_{L2}} \tag{19}$$

Equation 19 is applicable for locating any unbalanced fault such as a single line-to-ground, line-to-line, or double line-to-ground fault. However, during a three-phase balanced fault, negative-sequence components do not exist. In such a case, the same fault-locating principle is applied to a positive-sequence network and the distance to fault is computed as [19]

$$m = \frac{V_{G1} - V_{H1} + Z_{L1}I_{H1}}{(I_{G1} + I_{H1})\,Z_{L1}} \tag{20}$$

Note that there is no need to know the fault type. The presence or absence of negative-sequence components can be used to differentiate between an unbalanced or a balanced fault.

2) UNSYNCHRONIZED TWO-ENDED METHOD

Waveforms captured by IED devices at both ends of a transmission line may not be synchronized with each other. The GPS device may be absent or not functioning correctly. Alternatively, IEDs can have different sampling rates or they may detect the fault at slightly different time instants. The communication channel, which transfers data from one IED to the other, can also introduce a phase shift. Therefore, to align the voltage and current measurements of terminal G with respect to terminal H, the authors in [13] use a synchronizing operator $e^{j\delta}$ as,

Terminal G: $\quad V_{Fi} = V_{Gi}e^{j\delta} - mZ_{Li}I_{Gi}e^{j\delta}$ \hfill (21)

Terminal H: $\quad V_{Fi} = V_{Hi} - (1-m)Z_{Li}I_{Hi}$ \hfill (22)

where the subscript i refers to the ith symmetrical component. As discussed in the previous subsection, negative-sequence components are used to compute the location of an unbalanced fault while positive-sequence components are used to compute the location of a balanced three-phase fault. Equating (21) and (22), the synchronizing operator takes the form of

$$e^{j\delta} = \frac{V_{Hi} - (1-m)Z_{Li}I_{Hi}}{V_{Gi} - mZ_{Li}I_{Gi}} \tag{23}$$

Now, $e^{j\delta}$ can be eliminated from the fault location computation by taking the absolute value on both sides of (23) as

$$\left|e^{j\delta}\right| = 1 = \left|\frac{V_{Hi} - (1-m)Z_{Li}I_{Hi}}{V_{Gi} - mZ_{Li}I_{Gi}}\right| \tag{24}$$

Simplifying and rearranging the terms, the distance to fault m is a quadratic equation given by

$$m = \frac{-B \pm \sqrt{B^2 - 4AC}}{2A} \tag{25}$$

where the constants are defined as

$$A = |Z_{Li}I_{Gi}|^2 - |Z_{Li}I_{Hi}|^2$$
$$B = -2 \times \mathrm{Re}\left[V_{Gi}(Z_{Li}I_{Gi})^* + (V_{Hi} - Z_{Li}I_{Hi})(Z_{Li}I_{Hi})^*\right]$$
$$C = |V_{Gi}|^2 - |V_{Hi} - Z_{Li}I_{Hi}|^2$$

Solving the quadratic equation in (25) yields two values of m. The value between 0 and 1 per unit should be chosen as the location estimate.

3) UNSYNCHRONIZED CURRENT-ONLY TWO-ENDED METHOD

Due to limitations in data availability, suppose that only the current waveforms at terminals G and H are available for fault location purposes. Voltage phasors V_{G2} and V_{H2} are missing or simply not available. Using only the current and source impedance parameters, V_{F2} is calculated from either terminal as [20]

$$\text{Terminal G:} \quad V_{F2} = -(Z_{G2} + mZ_{L2})I_{G2} \tag{26}$$

$$\text{Terminal H:} \quad V_{F2} = -(Z_{H2} + (1-m)Z_{L2})I_{H2} \tag{27}$$

V_{F2} can be eliminated by equating (26) with (27). Also, to avoid any alignment issues with data sets from both ends of a transmission line, consider only the absolute values as

$$|I_{H2}| = \left|\frac{(Z_{G2} + mZ_{L2})}{(Z_{H2} + (1-m)Z_{L2})} \times I_{G2}\right| \tag{28}$$

Squaring and rearranging the terms, the distance to fault m can be solved by the quadratic equation in (25), where the constants are defined as

$$a + jb = I_{G2}Z_{G2}$$
$$c + jd = Z_{L2}I_{G2}$$
$$e + jf = Z_{H2} + Z_{L2}$$
$$g + jh = Z_{L2}$$
$$A = |I_{H2}|^2 \times \left(g^2 + h^2\right) - \left(c^2 + d^2\right)$$
$$B = -2 \times |I_{H2}|^2 (eg + fh) - 2(ac + bd)$$
$$C = |I_{H2}|^2 \times \left(e^2 + f^2\right) - \left(a^2 + b^2\right)$$

The value of m that lies between 0 and 1 per unit should be chosen as the final location estimate. This method is applicable for locating unbalanced faults only. The accuracy of location estimates depends on accurately knowing the source impedance parameters.

III. SOURCES OF ERROR IN IMPEDANCE-BASED FAULT LOCATION ALGORITHMS

As described in Section II, impedance-based fault location algorithms make certain simplifying assumptions when estimating the distance to a fault. Violation of these assumptions due to load, fault resistance, remote infeed, or mutual coupling all introduce error in the location estimates. In addition, when computing the distance to a fault, these fault-locating algorithms require the input of voltage and current phasors

during the fault as well as line impedance parameters. Inaccuracy in the input parameters further adds to the error in fault location. Three-terminal and tapped radial lines can also challenge the application of impedance-based algorithms. Therefore, this Section evaluates the sensitivity of fault-locating algorithms to the error sources mentioned above.
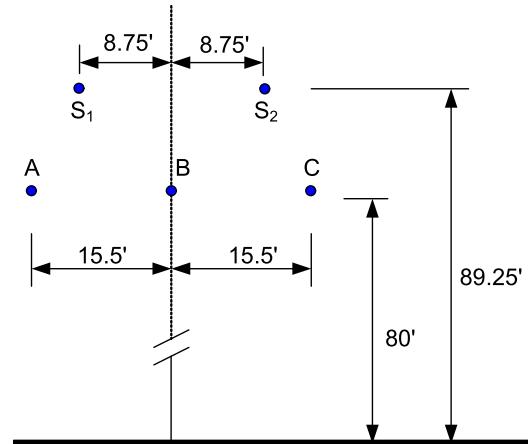

FIGURE 7. Tower Configuration of an Actual 69-kV Transmission Line.

A. DESCRIPTION OF THE 69-kV TEST CASE

To evaluate the sensitivity of impedance-based fault location algorithms to various sources of fault-locating error, the two-terminal transmission network shown in Fig. 1 was modeled in PSCAD simulation software [21]. The model will be used to replicate actual short-circuit faults that occur on a transmission line and generate the corresponding voltage and current waveforms. The rated voltage at terminals G and H is 69 kV. Relays, present at both terminals for line protection, record the three-phase line-to-ground voltages and currents at 128 samples per cycle. The network upstream from terminal G is represented by an ideal voltage source $E_G = 1\angle 10°$ per unit behind an equivalent positive- and zero-sequence impedance of $Z_{G1} = 3.75\angle 71°\,\Omega$ and $Z_{G0} = 11.25\angle 65°\,\Omega$, respectively. The network upstream from terminal H is also represented by an ideal voltage source $E_H = 1\angle 0°$ per unit behind an equivalent positive- and zero-sequence impedance of $Z_{H1} = 12\angle 71°\,\Omega$ and $Z_{H0} = 30\angle 65°\,\Omega$, respectively. The angle by which E_G leads E_H is known as the power angle (δ) and represents the net load served by the transmission line. The transmission line connecting terminals G and H is 18 miles long and was modeled using the frequency dependent model in PSCAD. The tower configuration of an actual 69-kV transmission line was used as shown in Fig. 7. Shield wires S_1 and S_2 protect phase conductors A, B, and C from direct lightning strikes. The material used to build the conductors is described in Table 2. Using Carson's equations [22] and an earth resistivity value of 100 Ω m, the positive- and zero-sequence line impedances were calculated to be $Z_{L1} = 15.55\angle 69.9°\,\Omega$ and $Z_{L0} = 35.46\angle 63.4°\,\Omega$, respectively.

TABLE 2. Conductor data.

	Material	Resistance (Ω/mi)	Diameter (inch)	GMR (feet)
Phase	ACSR Linnet 336,400 26/7	0.294	0.720	0.024
Shield	ACSR Grouse 80,000 8/1	1.404	0.367	0.009

Note that the test feeder has been intentionally designed to be simple, homogeneous, and compliant with all the assumptions made by impedance-based fault location algorithms. The goal is to introduce the fault-locating error sources one-by-one and study the impact on fault location estimates. Since a simple test system is being used, the error in location estimates is strictly proportional to the inaccuracies introduced. The analysis will, therefore, give an accurate measure of how significant a particular error source is and whether the error source should be considered for fault location purposes.
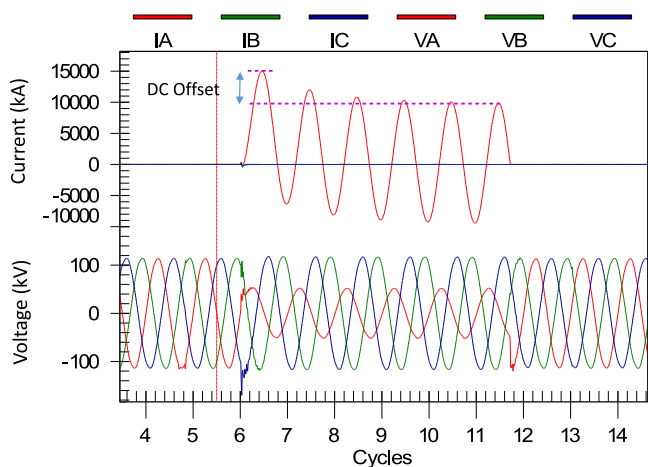

FIGURE 8. Fault Current with a Significant DC Offset.

B. DC OFFSET AND CT SATURATION

Impedance-based fault location algorithms employ phasor quantities of voltage and current to compute the distance to a fault. The calculation of these phasor quantities are complicated by the presence of an exponentially decaying DC offset which makes the fault current asymmetrical during the first few cycles as shown in Fig. 8. The asymmetry is maximum when a fault occurs at the zero-crossing of a voltage waveform and minimum when a fault occurs near the voltage peak. Fortunately, most single line-to-ground faults are caused by an animal or a tree coming into contact with a transmission line during peak voltage conditions [23]. In such cases, the DC offset is negligible. Faults due to lightning strikes are, however, random and can occur at any point on the voltage waveform, resulting in a significant asymmetry in the fault current.

To filter out the decaying DC offset and calculate the fault current phasor, Fast Fourier transforms (FFT) are commonly used [2]. A window length of one cycle is used to extract the fundamental-frequency magnitude and phase angle, and discard all harmonics. As an example, a rolling FFT filter
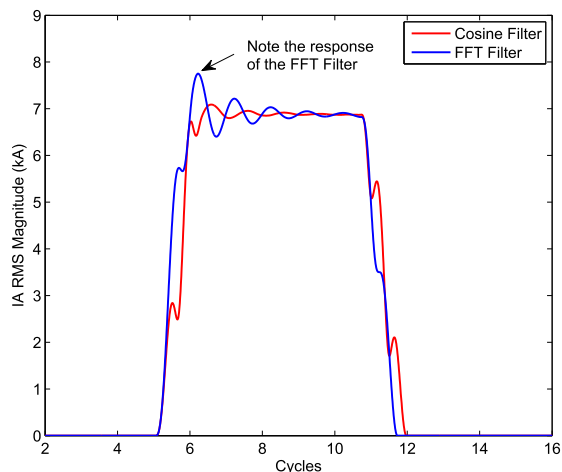

FIGURE 9. Comparing the Effectiveness of an FFT and a Cosine Filter in Filtering out the DC Offset.

is applied to the waveform in Fig. 8. In a rolling FFT, the FFT operation is performed repeatedly by a one-cycle long window sweeping across the entire waveform. As shown in Fig. 9, the FFT operation is successful in filtering out most, but not all of the DC offset. The RMS magnitude of the fault current fluctuates and reaches steady-state only when the DC offset decays. The corresponding variation in location estimates from the simple reactance method is shown in Fig. 10.
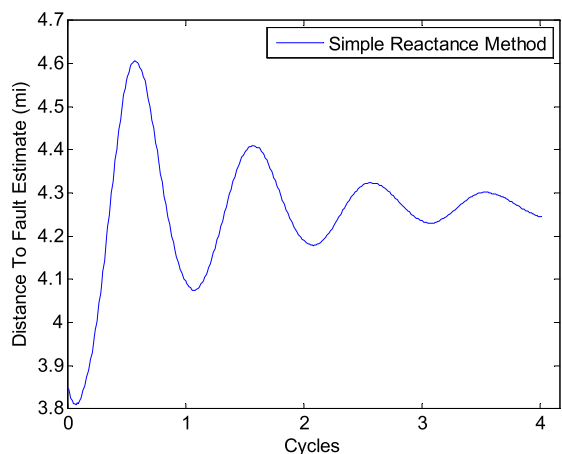

FIGURE 10. Variation in Location Estimates due to DC Offset. Voltage and Current Phasors were calculated using the FFT Filter.

Another phasor estimation technique, popularly used in Schweitzer relays, is the cosine filter [2]. Coefficients of this filter are sampled from a cosine wave and require a minimum response time of one and a quarter cycle. The quarter-cycle delay is used to calculate the phase angle. As seen in Fig. 9, the cosine filter does a better job of eliminating the DC offset than the FFT filter. The front and tail end of the signal are, however, severely distorted. This distortion offsets the accuracy of voltage and current phasor calculations during short-duration faults, resulting in erroneous location estimates.

In addition to DC offset, saturation of a current transformer (CT) can also distort fault current waveforms and introduce a

significant error in location estimates. CT saturation is often caused by fault currents having a significant DC offset [23]. As the DC offset decays down within two or three cycles, the CT may stop to saturate. Therefore, for faults which last for a number of cycles, the best way to handle CT saturation is to wait for the DC offset to decay before applying impedance-based fault location algorithms.

C. DELTA-CONNECTED POTENTIAL TRANSFORMERS
Impedance-based fault location algorithms require the input of line-to-ground voltages when computing the distance to a fault. When potential transformers are connected in a delta configuration, line-to-line voltages are available instead. The measured line-to-line voltages can be used by one-ended algorithms to estimate the location of line-to-line, double line-to-ground, or three-phase faults with no loss in accuracy. Line-to-ground voltages are, however, necessary to estimate the location of single line-to-ground faults [10]. If the zero-sequence impedance of the source, Z_{GO}, is available, then the line-to-ground voltage during the fault can be estimated as

$$V_{AF} = \frac{1}{3}(V_{AB} - V_{CA}) - Z_{G0}I_{G0} \qquad (29)$$

where V_{AF} is the estimated line-to-ground voltage of the faulted phase, V_{AB} is the line-to-line fault voltage measured between phases A and B, and V_{CA} is the line-to-line fault voltage measured between phases C and A. The accuracy of the estimated line-to-ground fault voltage depends on the accuracy of the zero-sequence source impedance.
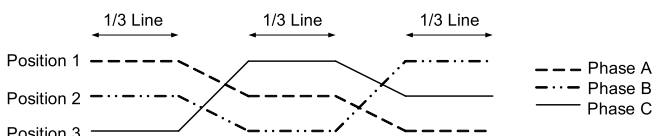

FIGURE 11. A Transposed Transmission Line [24].

D. UNTRANSPOSED LINES
Impedance-based fault location algorithms require the positive- and zero-sequence impedances of a transmission line to estimate the distance to a fault. When calculating the sequence line parameters, transmission lines are assumed to be transposed [22]. Transposition is the principle of physically exchanging the position of phase conductors at periodic intervals such that a particular conductor occupies all positions of a particular line configuration. This principle is illustrated in Fig. 11, where the positions of phase conductors A, B, and C are rotated every one-third of the total line length. Transposition equalizes the mutual coupling between the three phases and reduces the sequence impedance matrix, Z_{012}, to a diagonal matrix as shown in (30). The diagonal elements are formed by the sequence line impedances while the off-diagonal elements are zero, indicating that there is no

coupling between the sequence networks.

$$Z_{012} = \begin{bmatrix} Z_{L0} & 0 & 0 \\ 0 & Z_{L1} & 0 \\ 0 & 0 & Z_{L2} \end{bmatrix} \Omega \qquad (30)$$

Although line transposition is advantageous, it introduces complications in the design of a transmission line, and also increases the cost due to additional support structures and insulator string requirements. As a result, many transmission lines are not transposed. The sequence impedance matrix of an 18-mile long untransposed line having the line configuration shown in Fig. 7 is:

$$Z_{012} = \begin{bmatrix} 15.47 + j32.52 & 0.26 + j0.00 & 0.26 + j0.00 \\ 0.26 + j0.00 & 5.33 + j15.15 & 0.00 - j1.02 \\ 0.26 + j0.00 & 0.00 - j1.02 & 5.33 + j15.15 \end{bmatrix} \Omega$$

Observe that the off-diagonal elements are no longer zero. For example, $0.26 + j0.00\,\Omega$ represents the coupling between the positive- and zero-sequence network. Since impedance-based fault location algorithms assume the sequence networks to be decoupled from each other, an untransposed transmission line will affect the accuracy of location estimates.
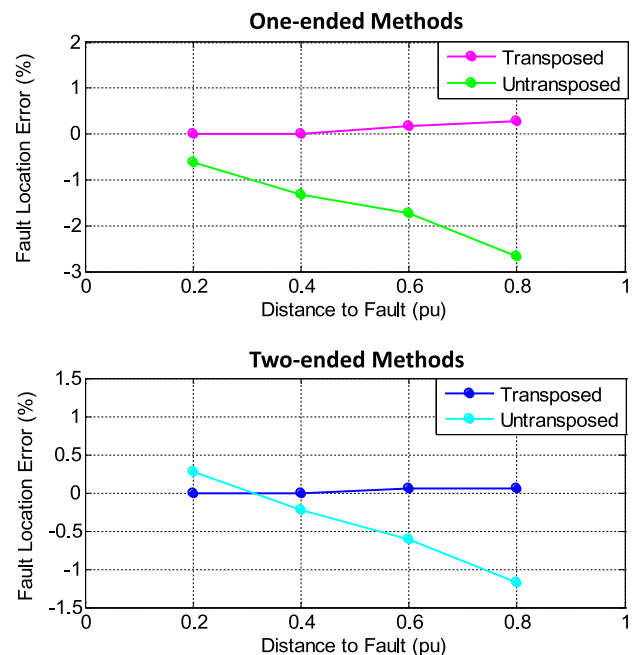

FIGURE 12. Error in Fault Location due to Untransposed Transmission Lines.

Fig. 12 demonstrates the impact of untransposed lines on one- and two-ended fault-locating techniques. In the reference case (transposed line), single line-to-ground faults were simulated along the length of the transmission line in the 69-kV test case with $R_F = 0\,\Omega$. Distances to faults were computed by applying one-ended methods to the voltage and current recorded at terminal G. To apply two-ended methods, measurements captured at both terminals were used. Next, the transmission line in the test case was intentionally changed to an untransposed line and faults were simulated with the same

value of R_F. Distances to faults were computed using the new set of voltage and current waveforms. The fault-location error was calculated as

$$\text{Error (\%)} = \frac{\text{Actual Location} - \text{Estimated Location}}{\text{Total Line Length}} \quad (31)$$

As seen in Fig. 12, because of the line transposition assumption, one-ended methods underestimate the location of a fault when compared against the reference case. The fault-location error increases as faults move farther away from the monitoring location. Two-ended methods are also affected by the line transposition assumption, the error being around 1.2%.

TABLE 3. Variation of earth resistivity with soil type [25].

Soil Type	Earth Resistivity (Ω m)	
	Range	Average
Peat	>1200	200
Adobe clay	2-200	40
Boggy ground	2-50	30
Gravel (moist)	50-3000	1000 (moist)
Sand and sandy ground	50-3000	200 (moist)
Stony and rocky ground	100-8000	2000
Concrete: 1 part cement + 3 parts sand	50-300	150

E. UNCERTAINTY IN EARTH RESISTIVITY

Earth resistivity ρ is the resistance with which the earth opposes the flow of electric current. It is an electrical characteristic of the ground and plays a critical role when calculating the zero-sequence impedance of a transmission line [22]. Determining the exact value of ρ is difficult since it varies greatly with the soil type as shown in Table 3. Most utilities use a standard earth resistivity value of $100\,\Omega$ m while others use the Wenner four-point method to measure ρ with great accuracy [18]. In addition to soil type, the value of ρ is also dictated by the moisture content in soils, temperature, and season of the year. Under extremely high or low temperatures, the soil is dry and has a very high earth resistivity value. During the rainy season, the value of ρ decreases. Minerals, salts, and other electrolytes make soils more conductive and tend to lower the earth resistivity value. Put another way, earth resistivity is never constant and is never known accurately.

TABLE 4. Effect of earth resistivity on line impedance parameters.

ρ (Ω m)	Z_{L1} (Ω)	Z_{L0} (Ω)	
10	$5.33 + j15.15$	$13.59 + j30.34$	
100	$5.33 + j15.15$	$15.47 + j32.53$	
500	$5.33 + j15.15$	$16.74 + j33.87$	
1000	$5.33 + j15.15$	$17.28 + j34.40$	

(ρ increases ↓ on left; Z_{L0} increases ↓ on right)

Table 4 shows the impact of a varying earth resistivity value on the positive- and zero-sequence impedances of the 69-kV transmission line described in Section III-A. The positive-sequence line impedance remains unaffected by changes in the value of earth resistivity. The zero-sequence line impedance, on the other hand, increases as ρ increases. Since one-ended fault location algorithms require the zero-sequence line impedance to compute the location of single
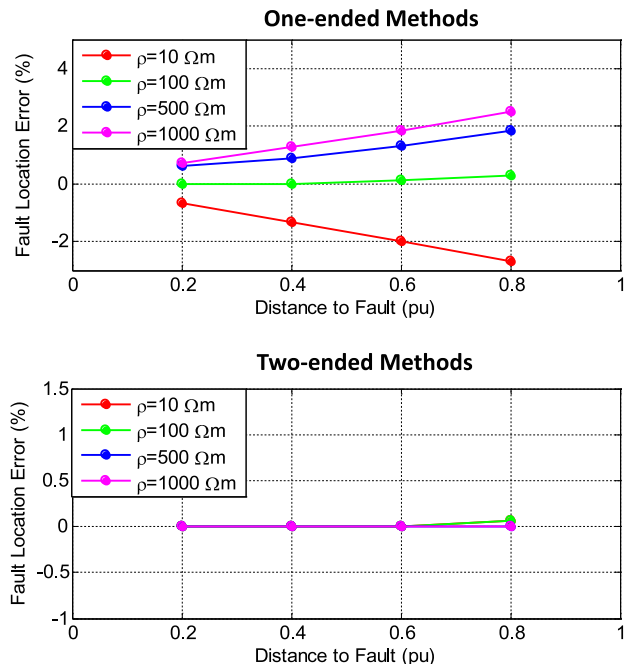

FIGURE 13. Error in Fault Location due to Uncertainty in Earth Resistivity.

line-to-ground faults, these methods are sensitive to any changes in earth resistivity.

As an example, the 69-kV test case was used to demonstrate the detrimental effect of ρ on one-ended methods. Single line-to-ground faults were simulated along the entire length of the transmission line with earth resistivity values ranging from 10 to $1000\,\Omega$ m. Line impedance parameters, used as an input to the fault location algorithms, were, however, calculated using the standard earth resistivity value of $100\,\Omega$ m. This case study reflects a practical scenario in which the resistivity of the soil can indeed vary over such a wide range. However, line impedance settings in a digital relay or a fault locator are computed using a particular value of ρ and do not reflect that change. As expected, the accuracy of one-ended methods are affected by the uncertainty in earth resistivity as shown in Fig. 13. When the actual value of earth resistivity is greater than the one used in the fault location computation, i.e., $100\,\Omega$ m, the distance to fault is overestimated. Similarly, when ρ is lower than the value used in the fault location computation, the distance to fault is underestimated. Also observe that the fault-location error increases linearly as the fault moves farther away from the monitoring location. This is because the error due to inaccurate zero-sequence line impedance adds up as the line length between the monitoring location and the fault increases. In contrast, two-ended methods do not use zero-sequence line impedance when estimating the distance to fault and are hence, not affected by any variation in ρ.

F. EFFECT OF SYSTEM LOAD

This subsection uses the 69-kV test case to investigate the impact of load on the accuracy of impedance-based fault location algorithms. Single line-to-ground faults were

simulated at several locations of the 18-mile long transmission line with different values of power angle δ and R_F. Recall that δ represents the net load served by the transmission network. One-ended fault location algorithms use voltage and current captured at terminal G while two-ended algorithms make use of waveforms captured at either line end.
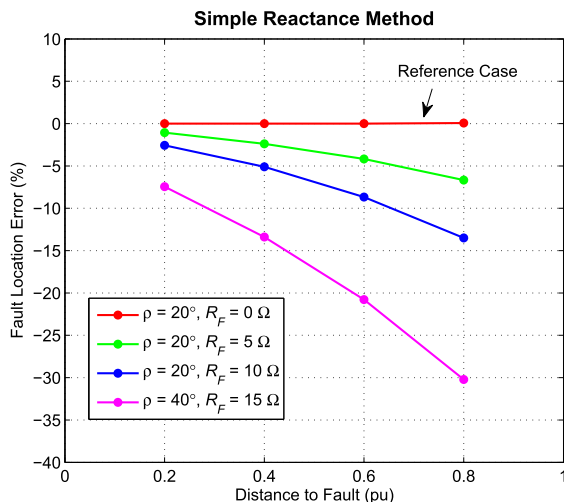

FIGURE 14. Reactance Error due to Load in Simple Reactance Method.

When the fault resistance is zero, location estimates from the simple reactance method are accurate, even under heavily loaded conditions as shown in Fig. 14. Note that a power angle of 20° corresponds to a load current of 430 A. For non-zero values of fault resistance, however, the same values of load current cause a reactance error in the simple reactance method. The reactance error is capacitive and the simple reactance method underestimates the location of faults. The fault-location error is further magnified when the load and fault resistance is increased to 40° and 15 Ω, respectively. It is also interesting to observe the increase in reactance error as the distance to fault increases in Fig. 14. When faults occur towards the end of the transmission line, the fault current contribution from the local terminal decreases. The load current constitutes a significant percent of the total fault current and increases the phase angle mismatch between I_F and I_G. For example, when a fault occurs at 0.8 per unit from terminal G, the load current is 28% of the fault current recorded at terminal G. As a result, the reactance error increases.

Takagi method uses the "pure fault" current to minimize the reactance error due to load. As shown in Fig. 15, the reactance error is negligible when $R_F = 10$ Ω and $\delta = 20°$. Modified Takagi, Eriksson, and two-ended methods are also not affected by an increase in the system load.

G. EFFECT OF A NON-HOMOGENEOUS SYSTEM

To demonstrate the effect of a non-homogeneous system on impedance-based fault location algorithms, the 69-kV test case was used. The test case is homogeneous since the local and remote source impedances have the same angle as the line impedance and hence, serves as the reference case.
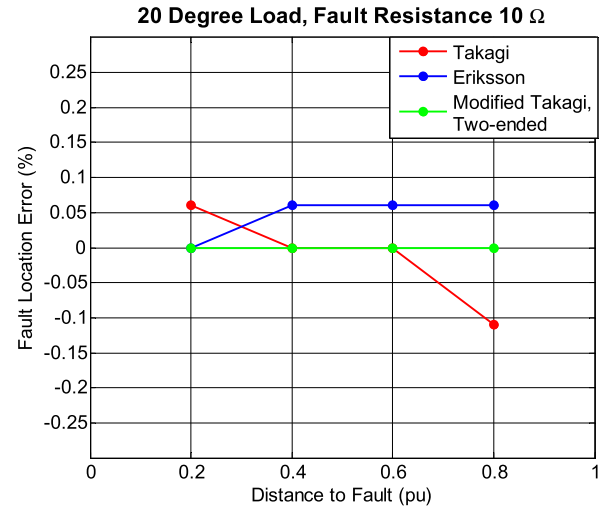

FIGURE 15. Load has no Impact on Takagi, Modified Takagi, Eriksson, and Two-ended Impedance-based Fault Location Algorithms.

Single line-to-ground faults were simulated along the entire length of the transmission line with $\delta = 1°$ and $R_F = 5$ Ω. To compute the location of faults, one-ended methods use voltage and current waveforms at terminal G while two-ended methods use voltage and current measurements at both terminals. Next, the system is intentionally made non-homogeneous by changing the value of Z_{G1} to $15\angle50°$ Ω. Faults were simulated using the same values of fault resistance and load. Location estimates from one and two-ended methods, computed using the new set of voltage and current measurements, were compared with those obtained in the reference case (homogeneous system) as shown in Fig. 16. As expected, the accuracy of simple reactance and Takagi methods deteriorate in a non-homogeneous system. The Eriksson method uses the remote source impedance to improve upon the performance of the Takagi method. The modified Takagi and two-ended methods are also robust to the increase in non-homogeneity and remain unaffected.

H. ZERO-SEQUENCE MUTUAL COUPLING

In transmission networks, it is common to find transmission lines that are physically parallel to each other. Two three-phase lines may be supported by the same tower or they may run on two separate towers but share the same right of way. Because of the mutual coupling between two lines, the impedance to fault calculation is influenced by currents flowing in the parallel line, thereby compromising the accuracy of location estimates.

As an example, consider the double-circuit transmission network shown in Fig. 17. Rated voltage at terminals G and H is 69 kV. Source impedance parameters Z_G and Z_H have the same values as those used in Section III-A. The transmission line is 18 miles long and has the configuration of an actual 69-kV double-circuit transmission line as shown in Fig. 18. Phase conductors A, B, and C represent Line 1 in Fig. 17 while phase conductors A', B', and C' represent Line 2.
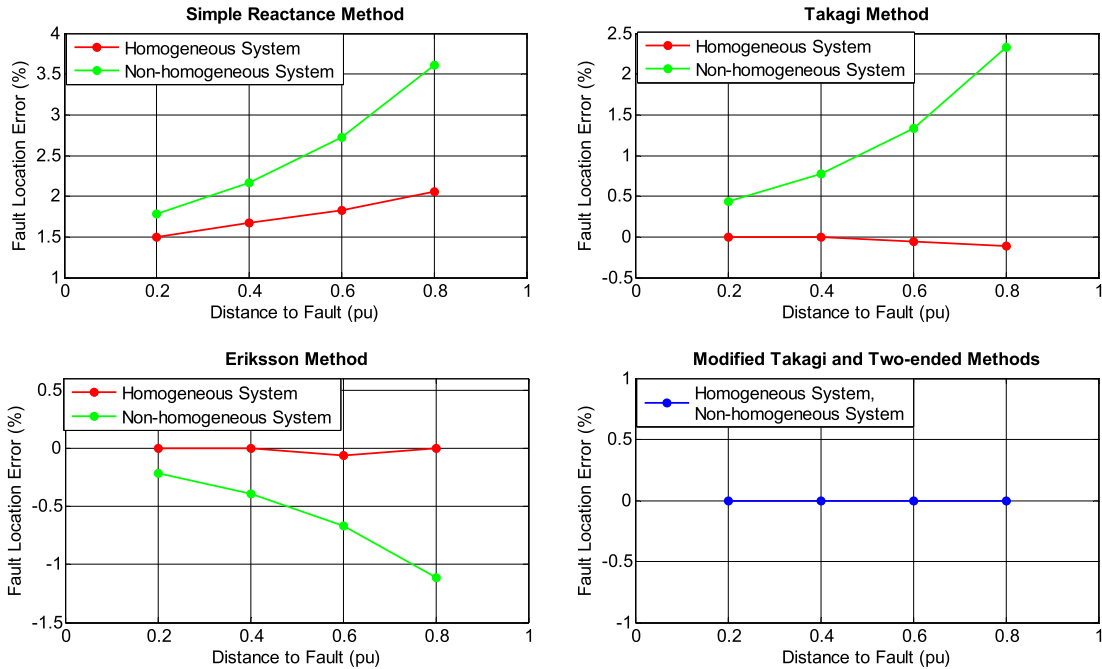
FIGURE 16. Effect of a Non-homogeneous System on Impedance-based Fault Location Algorithms.
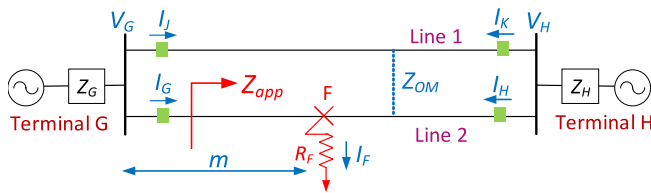

FIGURE 17. Double-circuit Transmission Network.

The material used to build the conductors is the same as those described in Table 2. Assuming both lines to be completely transposed and using an earth resistivity value of 100 Ω m, the sequence impedance matrix Z_{012} of the transmission line is shown in (32), as shown at the top of the next page. Here, the off-diagonal term $10.52 + j25.77$ Ω represents the zero-sequence mutual coupling (Z_{0M}) between two parallel lines and will always be present, regardless of whether the line is transposed or not. Observe that Z_{0M} is significant, around 63% of the zero-sequence line impedance.

Because of Z_{0M}, the apparent impedance measured at terminal G during a fault on Line 2 is modified and can be written as

$$Z_{app} = \frac{V_G}{I_G} = mZ_{L1} + mZ_{0M}\left(\frac{I_{J0}}{I_G}\right) + R_F\left(\frac{I_F}{I_G}\right) \quad (33)$$

where I_{J0} is the zero-sequence current in the parallel transmission line. If the two lines are parallel to each other for the entire line length, then Z_{0M} can be taken into consideration by simply measuring I_{J0} and inputting the value to (33). However, many different configurations of parallel lines are possible. For example, two lines may start parallel to each other from one terminal but end at two different terminals [26]. In such cases, the term $mZ_{0M}(I_{J0}/I_G)$ will
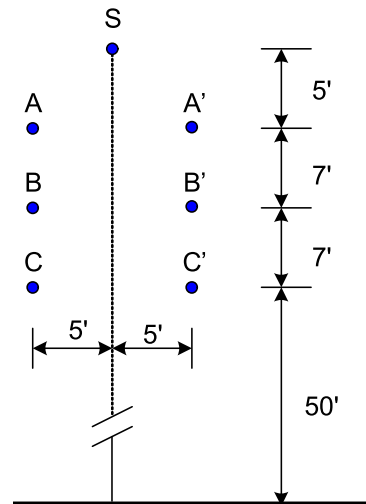

FIGURE 18. Configuration of an Actual 69-kV Double-circuit Transmission Line.

affect the fault location calculation. If the current I_G flows in the same direction as the current in the parallel line, I_J, then one-ended fault locating techniques will overestimate the location of the fault. On the other hand, if currents I_G and I_J flow in opposite directions, one-ended methods will underestimate the location of the fault [1].

To evaluate the impact of Z_{OM} on impedance-based fault location algorithms, the test case described in Fig. 17 was used. Analysis begins by first developing a reference case wherein there is no zero-sequence mutual coupling between the two lines. In reality, this is possible only when the two parallel lines are far apart from each other. Single line-to-ground faults were simulated at various locations of Line 2

$$Z_{012} = \begin{bmatrix} 15.82 + j40.91 & 0 & 0 & 10.52 + j25.77 & 0 & 0 \\ 0 & 5.33 + j12.92 & 0 & 0 & 0 & 0 \\ 0 & 0 & 5.33 + j12.92 & 0 & 0 & 0 \\ 10.52 + j25.77 & 0 & 0 & 15.82 + j40.91 & 0 & 0 \\ 0 & 0 & 0 & 0 & 5.33 + j12.92 & 0 \\ 0 & 0 & 0 & 0 & 0 & 5.33 + j12.92 \end{bmatrix} \Omega \quad (32)$$
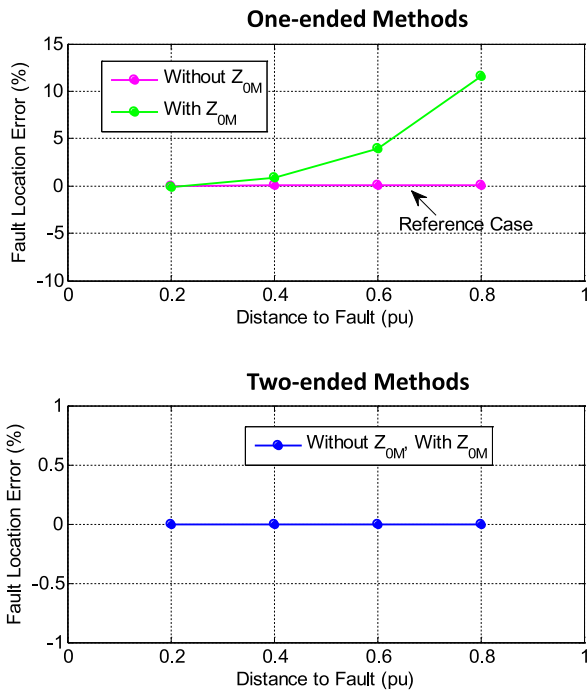

FIGURE 19. Impact of Zero-sequence Mutual Coupling on Impedance-based Fault Location Algorithms.

with $R_F = 0\ \Omega$ and a load angle of $\delta = 10°$. To compute the location of faults, one-ended methods use the voltage and current waveforms at terminal G while two-ended methods use waveforms at both ends of the line. Next, Z_{0M} was intentionally introduced in the base case and the same faults were simulated on Line 2. Location estimates computed using the new waveforms were then compared with those obtained in the reference case to obtain the increase in fault-locating error due to Z_{0M}. As shown in Fig. 19, all one-ended methods are equally affected by Z_{0M}. The increase in fault-locating error is around 10% at the far end of the line. Note that in this analysis, Z_{0M} was not compensated by I_{J0} in the parallel line.

The two-ended synchronized or the two-ended unsynchronized methods do not use the zero-sequence network when computing the distance to a fault. As a result, they are not affected by Z_{0M} as shown in Fig. 19. The unsynchronized current-only two-ended method is also not affected by Z_{0M}. However, this method does require the knowledge of negative-sequence currents I_{J2} and I_{K2} flowing in the parallel transmission line. This is because I_{J2} and I_{K2} cause an additional voltage drop across the source impedances Z_G and Z_H and if neglected, will cause an error in the location

estimates. Recall from Section II-B.3 that the unsynchronized current-only two-ended method solves for the distance to fault m by the quadratic equation given in (25). For double circuit lines, constants a and b change and are defined as follows:

$$a + jb = I_{G2}Z_{G2} + I_{J2}Z_{G2} - I_{K2}Z_{H2}$$

The other constants remain the same. It is also worth mentioning that the unsynchronized current-only two-ended method is not affected by the different possible configurations of parallel transmission lines.
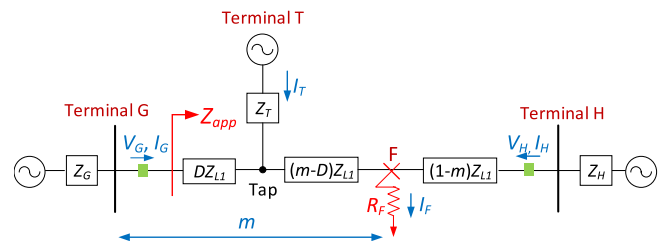

FIGURE 20. Three Terminal Transmission Line.

I. THREE-TERMINAL LINES

Impedance-based fault location algorithms in Section II have been primarily developed for a two-terminal transmission line. The application scenario changes in the case of a three-terminal line as shown in Fig. 20. One-ended fault location algorithms are accurate up to the tap point only. When a fault occurs beyond the tap point, the fault current contributed by the third terminal modifies the impedance to fault equation and results in a significant error in location estimates. For example, consider the fault shown in Fig. 20. The apparent impedance measured from terminal G is:

$$Z_{app} = \frac{V_G}{I_G} = mZ_{L1} + (m - D)Z_{L1}\frac{I_T}{I_G} + R_F\left(\frac{I_F}{I_G}\right) \quad (34)$$

where I_T is the fault current contributed by terminal T and D is the distance of the tap point from terminal G. Since one-ended algorithms at terminal G have no knowledge about I_T, the term $(m - D)Z_{L1}(I_T/I_G)$ will cause one-ended methods to overestimate the location of the fault. Moreover, current I_F is the summation of I_G, I_H, and I_T. As a result, I_F and I_G have different phase angles in a non-homogeneous system and will introduce an additional reactance error. Depending on whether the reactance error is inductive or capacitive, distance to fault is over or underestimated. On the other hand, one-ended methods can successfully estimate the location of fault F when applied from terminal H. Since the fault

is located before the tap point, the fault current contributed by terminals G and T act as remote infeed only and do not alter the apparent impedance measured from terminal H. Therefore, the solution in the case of three-terminal lines is to apply one-ended methods from each terminal. One of the three estimates will successfully pinpoint the exact location of the fault as demonstrated in the case study described in Section IV-C.

Two-ended algorithms can be extended for application to three-terminal lines with certain additional modifications. For instance, authors in [20] transform a three-terminal line into an equivalent two-terminal line and then apply the unsynchronized current-only two-ended method.
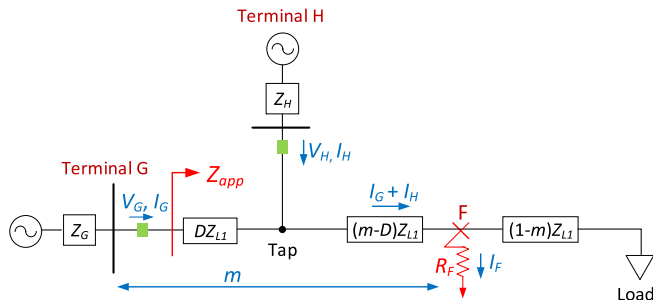

FIGURE 21. Fault on a Radial Feeder Tapped from a Two-terminal Line.

J. TAPPED RADIAL LINE
Locating faults on a radial feeder tapped from a two-terminal transmission line is a challenging task for impedance-based fault location algorithms. When a fault occurs in the line section between the tap point and the load, as illustrated by F in Fig. 21, the apparent impedance measured from terminal G is the same as that given by (34). One-ended algorithms make use of measurements captured at only one end of the line. Therefore, neglecting the fault current contributed by terminal H will cause one-ended methods to overestimate the fault location.

Measurements captured at both ends of a line can be used to improve the accuracy of location estimates. The first step is to confirm whether the fault is located on the radial line. This is achieved by calculating the voltage at the tap point during fault, V_{Tap}, from terminals G and H as shown below:

Terminal G: $V_{Tap} = V_G - DZ_{L1}I_G$ (35)

Terminal H: $V_{Tap} = V_H$ (36)

If the fault is on the radial line, V_{Tap} calculated from terminal G will be equal to that calculated from terminal H. This is because terminals G and H operate in parallel to feed the fault on the radial line. Next, (34) can be used to compute the distance to fault.

IV. APPLICATION OF IMPEDANCE-BASED FAULT LOCATION ALGORITHMS TO FIELD DATA
This Section demonstrates the application of impedance-based fault location algorithms on actual fault event data

captured in utility transmission networks. Data consists of voltage and current waveforms recorded by digital fault recorders at both ends of a transmission line, line impedance parameters, and known location of the fault. Each event was chosen to highlight a specific aspect of impedance-based fault location and to illustrate the potential benefits of IED data.
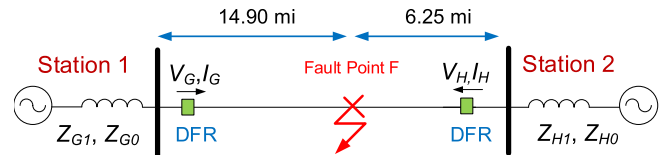

FIGURE 22. Event 1 is a A-G Fault Located 14.90 miles from Station 1 or 6.25 miles from Station 2.

A. TRANSMISSION SYSTEM FAULT EVENT 1
On 27 April 2012 at 00:48 am, a single line-to-ground fault occurred on phase A of a 161-kV transmission line. The transmission line experiencing fault is 21.15 miles long and connects Station 1 with Station 2 as shown in Fig. 22. The positive- and zero-sequence impedances of the line are $Z_{L1} = 3.18 + j16.68\ \Omega$ and $Z_{L0} = 15.21 + j52.45\ \Omega$, respectively. The fault was caused by a failed line arrestor located 14.90 miles from Station 1 or 6.25 miles from Station 2.
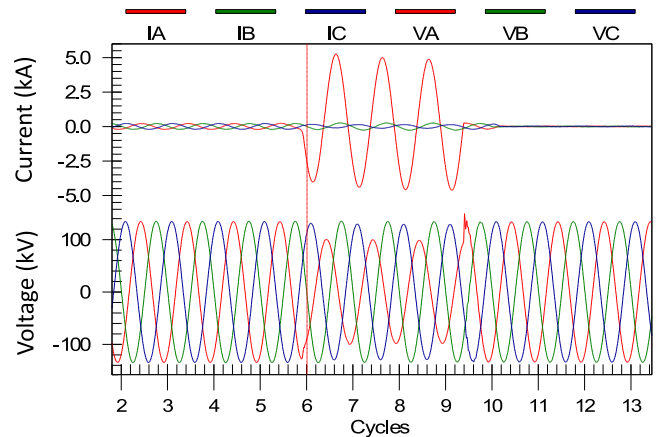

FIGURE 23. Event 1 DFR Measurements at Station 1. Phase A has a Fault Current Magnitude of 3.4 kA.

Digital fault recorders (DFRs) at both stations record the three-phase line-to-ground voltage and current waveforms at 100 samples per cycle as shown in Fig. 23 and Fig. 24. Before the fault, Station 1 supports a load current of 150 A and Station 2 supports a load current of 130 A. During the fault, the current magnitude in the faulted phase increases to 3.4 kA at Station 1 and to 6.1 kA at Station 2. Note that to calculate the fault current at Stations 1 and 2, the third cycle after fault was chosen as the best cycle to perform the FFT operation.

To estimate the distance to fault, one-ended impedance-based fault location algorithms were applied from Station 1 and Station 2. The modified Takagi and Eriksson methods
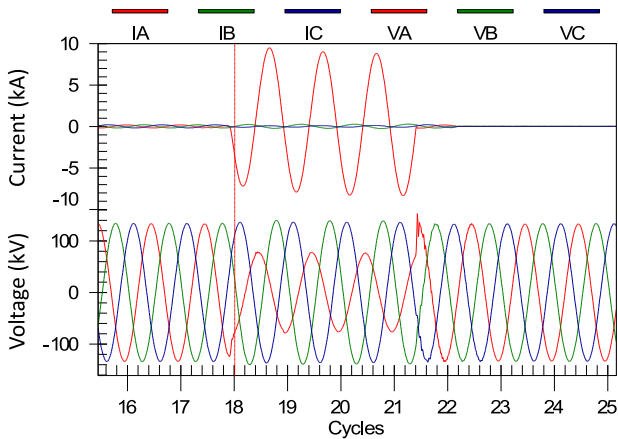
FIGURE 24. Event 1 DFR Measurements at Station 2. Phase A has a Fault Current Magnitude of 6.1 kA.

require source impedance parameters as an additional input when computing the fault location. Therefore, waveform data at Station 1 were used in (15) and (10) to estimate the positive- and zero-sequence source impedances at Station 1 to be $Z_{G1} = 9.4\angle89°\,\Omega$ and $Z_{G0} = 6.1\angle90°\,\Omega$, respectively. In a similar manner, the positive- and zero-sequence source impedances at Station 2 were estimated to be $Z_{H1} = 6.1\angle90°\,\Omega$ and $Z_{H0} = 8.8\angle81°\,\Omega$, respectively. As shown in Table 5, location estimates from one-ended methods are in agreement with those estimated by the DFRs and are close to the actual location of the fault.

TABLE 5. Event 1 location estimates from one-ended methods.

Station	Actual Location (mi)	DFR (mi)	Estimated Location (mi)			
			Simple Reactance	Takagi	Modified Takagi	Eriksson
1	14.90	14.40	14.78	14.77	14.77	14.77
2	6.25	6.40	6.38	6.36	6.36	6.36

In addition to one-ended methods, two-ended fault location methods were also used to estimate the distance to fault. Measurements from both ends of the transmission line are unsynchronized due to a difference in the fault trigger time. As a result, the unsynchronized two-ended method was used. Distance to fault was computed to be 14.76 miles from Station 1 as shown in Table 6.

TABLE 6. Event 1 location estimate from two-ended methods.

Station	Actual Location (mi)	Estimated Location (mi)
1 and 2	14.90	14.76

In summary, this case study demonstrates the success of both one- and two-ended algorithms in tracking down the exact location of the fault. To further increase the benefits of fault-locating, fault event data captured at Station 1 and

Station 2 were used to estimate the value of fault resistance. Substituting the known value of *m* in (14), the fault resistance from Station 1 was estimated to be 0.19 Ω. Similarly, the fault resistance from Station 2 was estimated to be 0.16 Ω. The accuracy of the estimated fault resistance can be ascertained from the fact that the simple reactance method in Table 5 did not suffer from reactance error due to load current. The absence of any reactance error is indicative that the fault resistance is indeed negligible in this event.
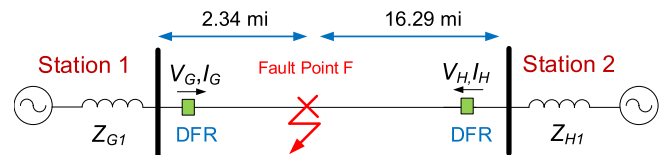

FIGURE 25. Event 2 is a AB Fault Located 2.34 miles from Station 1 or 16.29 miles from Station 2.

B. TRANSMISSION SYSTEM FAULT EVENT 2

Event 2 is a line-to-line fault that occurred between phases A and B of a 161-kV transmission line on 25 March 2012 at 03:56 pm. The transmission line is 18.63 miles long and connects Station 1 with Station 2 as shown in Fig. 25. The positive- and zero-sequence impedances of the line are $Z_{L1} = 2.39 + j12.81\,\Omega$ and $Z_{L0} = 9.95 + j40.70\,\Omega$, respectively and will be utilized for fault location purposes. The root-cause of the fault was a tree falling on the transmission line 2.34 miles from Station 1 or 16.29 miles from Station 2.
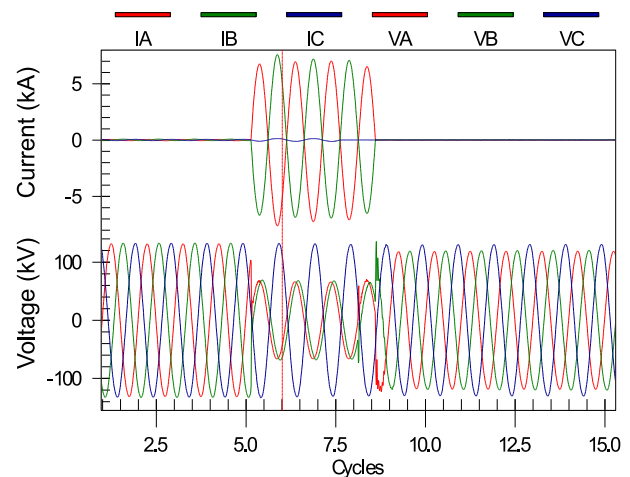
FIGURE 26. Event 2 DFR Measurements at Station 1. Fault Current Magnitude in Phases A and B is 4.8 kA.

Digital fault recorders (DFRs) at both ends of the transmission line capture voltage and current waveforms during the fault at 100 samples per cycle. The waveforms are shown in Fig. 26 and Fig. 27, and can be used to reconstruct the sequence of events. Before the fault, Station 1 and Station 2 support a load current of 47 A and 55 A, respectively. When a fault occurs 2.34 miles from Station 1, the DFR at Station 1 measures a fault current of 4.8 kA in phases A and B.

After 3.5 cycles, a protective relay at Station 1 initiates a fast trip operation. Station 2, on the other hand, continues to feed the fault for 34.5 cycles. During the first 3.5 cycles, when both stations are feeding the fault, the DFR at Station 2 records a current magnitude of 3.2 kA in the faulted phases. This is marked as "Part 1" in Fig. 27. After 3.5 cycles, when Station 1 trips offline, the fault current from Station 2 increases to 4 kA as indicated by "Part 2" in Fig. 27. After 34.5 cycles, the recloser at Station 2 operates to allow the fault to clear out on its own. The reclose interval is 2.07 seconds. The fault is, however, permanent in nature. As a result, when the recloser closes back into the transmission line, the fault is still present and the DFR at Station 2 records a fault current magnitude of 4 kA as illustrated by "Part 3" in Fig. 27. The recloser finally locks out after 3.5 cycles.

FIGURE 27. Event 2 DFR Measurements at Station 2.

TABLE 7. Event 2 location estimates from one-ended methods.

Station	Actual Location (mi)	DFR (mi)	Estimated Location (mi)		
			Simple Reactance	Takagi	Eriksson
1	2.34	3.90	3.77	3.77	3.78
2, Part 2	16.29	18.00	18.08	18.08	18.04
2, Part 3			18.18	18.18	18.16

To track down the location of the permanent fault, one-ended impedance-based fault location algorithms were applied from Station 1. Location estimates are, however, not accurate and exceed the actual location of the fault by 1.4 miles as shown in Table 7. One-ended fault location algorithms were then applied to "Part 2" and "Part 3" of the waveforms captured at Station 2. This is because in "Part 2" and "Part 3", only Station 2 contributes current to the fault. There is no remote infeed from Station 1 and hence, location estimates are expected to have a high degree of accuracy. Unfortunately, as seen in Table 7, one-ended methods from Station 2 also overestimate the location of the fault by 1.9 miles. It should be noted that in addition to the one-ended methods, the DFRs at Station 1 and Station 2 also incorrectly identify the location of the fault. To explain the fault location error, recall that the Eriksson method is robust to fault resistance, load, and a non-homogeneous system. Erroneous estimates from the Eriksson method, therefore, rules

out the above sources of fault-locating error. Moreover, since the fault does not involve the ground, zero-sequence mutual coupling and uncertainty in zero-sequence line impedance can also be eliminated as potential error sources. Additional information regarding the transmission network is required to identify the factor responsible for the error in fault location.

TABLE 8. Event 2 location estimate from two-ended methods.

Station	Actual Location (mi)	Estimated Location (mi)
1 and 2	2.34	2.46

The fault location estimate from the unsynchronized two-ended method is summarized in Table 8. This two-ended method was chosen since the DFRs at Stations 1 and 2 have different fault trigger times and was applied to that part of the waveform wherein both stations are contributing to the fault, i.e., Station 1 and "Part 1" of Station 2 waveform. As seen from the table, the location estimate from the two-ended method show a significant improvement over one-ended methods and is within 0.15 miles of the actual fault location.

TABLE 9. Estimated positive-sequence source impedances.

Station	Source Impedance (Ω)
1	$1.85 + j14.46$
2, Part 1	$4.25 + j12.80$
2, Part 2	$6.46 + j6.29$
2, Part 3	$3.19 + j7.22$

In addition to estimating the location of the fault, voltage and current waveforms captured during the fault provide valuable feedback about the state of the transmission network upstream from the DFR at Station 1 and Station 2. For example, to implement the Eriksson method in Table 7, waveform data at each individual station were used in (15) to estimate the source impedance parameters as listed in Table 9. Observe the sudden change in the positive-sequence source impedance at Station 2 from "Part 1" to "Part 2". Keep in mind that the fault current contribution from Station 2 lasts for 34.5 cycles. Several generators upstream from Station 2 must have switched offline during this long time frame, resulting in a sharp decrease in the source impedance.

C. TRANSMISSION SYSTEM FAULT EVENT 3

On 14 September 2011 at 6:23 pm, a double line-to-ground fault occurred between phases A and B of a 161-kV transmission line. The fault was caused by a lightning strike during stormy weather conditions. The transmission line experiencing fault is 46.25 miles long and connects Station 1 with Station 2 as shown in Fig. 28. The positive- and zero-sequence impedances of the transmission line are $Z_{L1} = 7.26 + j36.70 \ \Omega$ and $Z_{L0} = 29.34 + j108.24 \ \Omega$, respectively. The actual location of the fault was reported by the utility to be 29.49 miles from Station 1 or 16.76 miles from Station 2.

FIGURE 28. Event 3 is a AB-G Fault, 29.49 miles from Station 1 or 16.76 miles from Station 2.

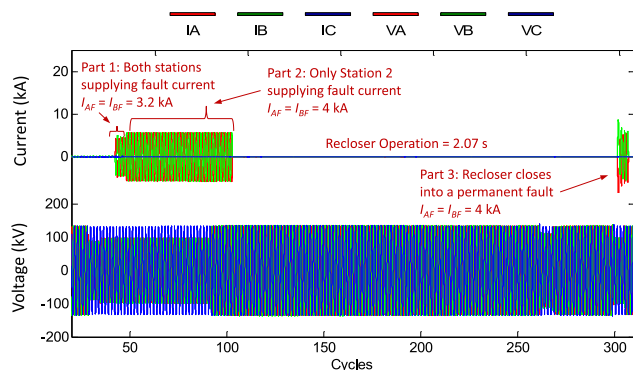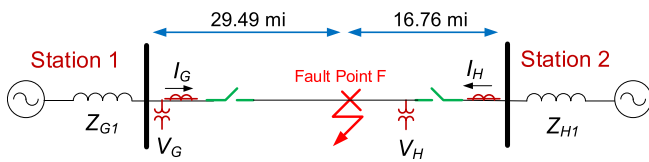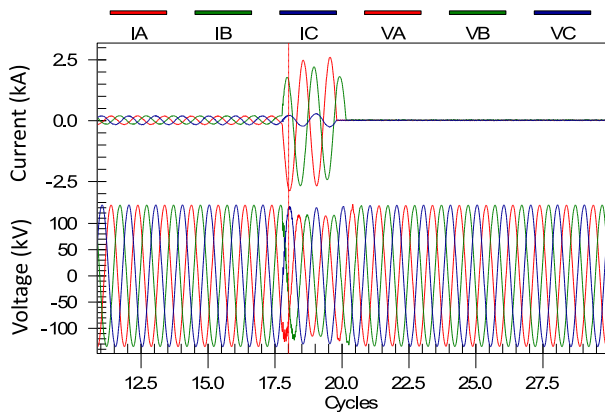**FIGURE 29.** Event 3 DFR Measurements at Station 1. Phases A and B have a Fault Current Magnitude of 1.9 kA.
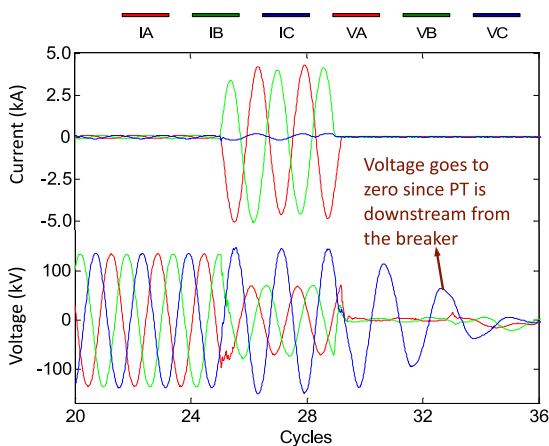

FIGURE 30. Event 3 DFR Measurements at Station 1. Phases A and B have a Fault Current Magnitude of 3.2 kA.

A digital fault recorder (DFR), present at Station 1, records the voltage and current waveforms during the fault at 100 samples per cycle as shown in Fig. 29. A DFR at Station 2 also records the voltage and current waveforms at 96 samples per cycle as shown in Fig. 30. Prefault currents from Station 1 and 2 are 120 A and 70 A, respectively. During the fault, Station 1 records a current magnitude of 1.9 kA in phases A and B, and Station 2 records a current magnitude of 3.2 kA in the faulted phases. After 2.5 cycles, the fault is cleared by the operation of a circuit breaker at either line end. Since this is a short-duration fault, the FFT operation was performed on the second cycle to minimize the effect of DC offset in calculating the fault current phasor. Also observe that

the voltage at Station 2 goes to zero once the fault is cleared from the circuit. This indicates that the voltage measurements are captured by a line PT downstream from the breaker as shown in Fig. 28.

TABLE 10. Event 3 location estimates from one-ended methods.

Station	Actual Location (mi)	DFR (mi)	Estimated Location (mi)		
			Simple Reactance	Takagi	Eriksson
1	29.49	49.10	49.27	49.43	49.65
2	16.76	16.60	16.68	16.66	16.65

Table 10 lists the distance to fault estimates from one-ended fault location algorithms. Source impedances at Stations 1 and 2, required as an input to the Eriksson method, were estimated using (15) to be $Z_{G1} = 9.6\angle86°\Omega$ and $Z_{H1} = 14.5\angle85°\Omega$, respectively. As shown in Table 10, one-ended fault location techniques are successful in pinpointing the exact location of the fault from Station 2. The same fault-locating algorithms, however, overestimate the location of the fault from Station 1. The actual location of the fault is 29.49 miles from Station 1 while one-ended methods estimate the distance to be around 49.65 miles. The location estimate from the DFR at Station 1 also show a considerable error of 19.6 miles.

In an effort to improve the accuracy of location estimates, two-ended fault location techniques were implemented using measurements from both ends of the transmission line. Since the DFRs at Station 1 and 2 have different sampling rates, measurements are not synchronized. Therefore, the unsynchronized two-ended method was used. Surprisingly, the location estimate from the two-ended method also show a considerable fault-location error of 8 miles as shown in Table 11.

TABLE 11. Event 3 location estimate from two-ended methods.

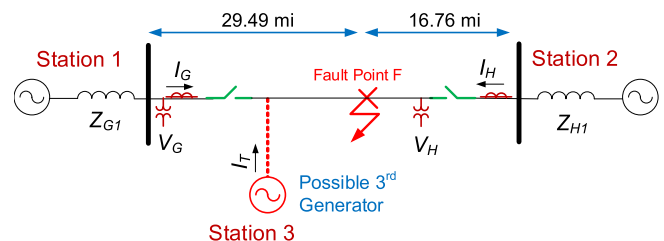| Station	Actual Location (mi)	Estimated Location (mi)
1 and 2	29.49	37.41

FIGURE 31. A Third Station is Suspected to be Present Between Station 1 and the Fault.

To explain the error in fault location from Station 1, recall that two-ended methods are robust to fault resistance, load current, non-homogeneous system, zero-sequence

TABLE 12. Summary of input data requirements of impedance-based fault location algorithms.

Input Data	Simple Reactance	Takagi	Modified Takagi	Eriksson	Novosel et al.	Synchronized Two-ended	Unsynchronized Two-ended	Unsynchronized Current-only Two-ended
Fault Event Data								
Fault Type	✓	✓	✓	✓	✓			
Fault Voltage,[1] Current Phasor (Local End)	✓	✓	✓	✓	✓	✓	✓	✓
Fault Voltage Phasor[1] (Remote End)						✓	✓	
Fault Current Phasor (Remote End)						✓	✓	✓
Synchronized Data						✓		
Prefault Current Phasor		✓		✓	✓			
Prefault Voltage Phasor					✓			
Transmission Line Parameters								
Line Length	✓	✓	✓	✓	✓	✓	✓	✓
Positive-sequence Line Impedance	✓	✓	✓	✓	✓	✓	✓	✓
Zero-sequence Line Impedance	✓	✓	✓	✓	✓			
Source Impedance Parameters								
Positive-sequence Source Impedance (Local End)				Optional	Optional			
Positive-sequence Source Impedance (Remote End)			✓					
Negative-sequence Source Impedance (Local End)								✓
Negative-sequence Source Impedance (Remote End)								✓
Zero-sequence Source[2] Impedance (Local End)			Optional					
Zero-sequence Source Impedance (Remote End)			✓					

[1] Voltages measured between the line and the ground.

[2] If line-to-line voltages are available instead of line-to-ground voltages, then the zero-sequence source impedance at the local end is necessary to estimate the line-to-ground voltage of the faulted phase during a single line-to-ground fault as given by (29).

mutual coupling, and an uncertain value of zero-sequence line impedance. Therefore, the above sources of fault-locating error were ruled out. Furthermore, since the one-ended location estimates from Station 2 are accurate, it is reasonable to assume that the positive-sequence line impedance is also accurate. The fact that the distance to fault from Station 1 was overestimated indicates a strong possibility of a third generating station between Station 1 and the fault as illustrated in Fig. 31. The fault current from Station 3, I_T, increases the apparent impedance measured at Station 1. As a result, one- and two-ended algorithms overestimate the location of the fault from Station 1. As discussed in Section III-I, in a three-terminal line, one-ended fault location estimates computed from only one of the three terminals, Station 2 in this case, is accurate.

As an added benefit to fault-locating, waveforms at Station 2 were used in (14) to estimate the fault resistance as

0.87 Ω. Waveforms from Station 1 were not used since the fault current from Station 3 modifies the fault resistance calculation.

V. LESSONS LEARNED

This paper reviews one- and two-ended impedance-based fault location algorithms that are used to locate faults in a transmission network. The simple reactance method is the most straightforward of all fault location algorithms. The accuracy of this method, however, deteriorates due to fault resistance, load current, and remote infeed in a non-homogeneous system. Subsequent fault-locating algorithms have been developed to address the above sources of error. For example, the Takagi method is robust to load but sensitive to remote infeed. The modified Takagi and Eriksson methods use source impedance parameters to eliminate any error caused by load and remote infeed. Additional sources

TABLE 13. Summary of fault-locating error sources that affect impedance-based fault location algorithms.

Input Data	Simple Reactance	Takagi	Modified Takagi	Eriksson	Novosel et al.	Synchronized Two-ended	Unsynchronized Two-ended	Unsynchronized Current-only Two-ended
Instrument Transformer Challenges								
Loss of Potential	✓	✓	✓	✓	✓	✓	✓	
CT Saturation	✓	✓	✓	✓	✓	✓	✓	✓
Delta-connected[1] Potential Transformers	✓	✓	✓	✓	✓	✓	✓	
Power System Challenges								
System Load	✓							
Non-homogeneous System	✓	✓						
Parallel Lines[2] (Mutual Coupling)	✓	✓	✓	✓	✓			✓
Fault Related Challenges								
Fault Resistance	✓	✓						
Fault Incidence Angle (DC Offset)	✓	✓	✓	✓	✓	✓	✓	✓
Application Related Challenges								
Two-terminal Lines	✓	✓			N/A			
Soil Type, Weather[3] Temperature, Season (Earth Resistivity)	✓	✓	✓	✓	✓			
Untransposed Lines	✓	✓	✓	✓	✓	✓	✓	✓
Tapped Lines[4]	✓	✓	✓	✓	✓	✓	✓	✓
Three-terminal Lines[4]	✓	✓	✓	✓	✓	✓	✓	✓

[1] Delta-connected PTs pose a problem in locating single line-to-ground faults only. If the zero-sequence impedance of the local source is available, estimate the corresponding line-to-ground voltages.

[2] Mutual coupling affects the accuracy of one-ended algorithms in locating single line-to-ground faults only. If transmission lines are parallel for the entire line length, then the residual current from the parallel line can improve the accuracy of one-ended methods. The unsynchronized current-only two-ended method, however, requires the negative-sequence currents at both ends of the parallel line for all fault types.

[3] Earth resistivity affects the accuracy of locating single line-to-ground faults only.

[4] It is possible to modify two-ended methods for application to tapped lines and three-terminal lines.

of error that compromise the accuracy of one-ended algorithms in locating single line-to-ground faults are mutual coupling in double-circuit transmission lines and an uncertain value of zero-sequence line impedance. Two-ended fault-locating algorithms use measurements from both ends of a transmission line to overcome all the short-comings of one-ended methods and are attractive for tracking down the exact location of a fault. Unfortunately, measurements captured at the remote end of the line are not always available. Therefore, data availability is one of the most important criteria for selecting the best approach for fault location. Table 12 summarizes the input data requirements of all impedance-based fault location algorithms.

Identifying the best approach for fault location also depends on the application scenario. For example, location estimates from two-ended algorithms are not always accurate as in the case of three-terminal lines demonstrated in Section IV-C. In contrast, one-ended fault locating algorithms applied from one of the three terminals pinpoints the exact location of the fault. The two-ended fault location algorithm failed not because of limitations in the algorithm but because it was not meant for use in a three-terminal line. Therefore, when implementing fault location algorithms, users should be aware of the application scenario, identify possible error sources, and then choose the algorithm that is robust to those error sources. Table 13 summarizes the error sources that affect the accuracy of impedance-based fault location algorithms.

Knowing the fault location application scenario is also useful in identifying what additional equipment needs to be installed for improving the accuracy of fault location algorithms. For instance, locating faults on a radial line tapped from a multi-ended transmission line is a complex problem as discussed in Section III-J. Placing an additional monitor at the tap point in Fig. 21 would drastically simplify impedance-based fault location.

In addition to computing the location of a fault, this paper demonstrates the other potential benefits of event reports

captured by intelligent electronic devices (IEDs) during a fault. For example, fault event data can be used to determine the Thevenin impedance upstream from the IED device. The estimated Thevenin impedance can yield valuable clues about the response of the upstream transmission network during the fault, including whether any generators have tripped offline. Fault event data can also be used to estimate the value of fault resistance, which is useful for identifying the root cause of the fault and also for validating system modeling parameters.

In summary, the paper recommends the following criteria for selecting the most suitable fault location algorithm: (a) data availability, and (b) fault location application scenario. Utility operators should also remember that when estimating the distance to a fault, fault location algorithms assume that only one fault occurs in the transmission line at a given point in time and that the location of the fault remains the same for the entire duration of the fault-locating window. Faults caused by animal or tree contact with a transmission line, or insulation failure in power system equipment have one single location. However, when lightning strikes an overhead line or a shield wire, the voltage across the insulator is so large that it causes a back flash-over and a fault. This overvoltage may propagate to the neighboring towers and cause simultaneous flash-overs at several locations. In this case, the fault is not limited to one single location and can challenge the application of impedance-based fault location algorithms.

ACKNOWLEDGMENT

REFERENCES

[1] *IEEE Guide for Determining Fault Location on AC Transmission and Distribution Lines*, IEEE Standard C37.114-2004, 2005, pp. 1–36.

[2] *Distribution Fault Location: Field Data and Analysis*, EPRI, Palo Alto, CA, USA, Tech. Rep. 1012438, 2006.

[3] S. Lotfifard, M. Kezunovic, and M. J. Mousavi, "A systematic approach for ranking distribution systems fault location algorithms and eliminating false estimates," *IEEE Trans. Power Del.*, vol. 28, no. 1, pp. 285–293, Jan. 2013.

[4] M. M. Saha, R. Das, P. Verho, and D. Novosel, "Review of fault location techniques for distribution systems," in *Proc. Power Syst. Commun. Infrastruct. Future*, Sep. 2002.

[5] J. Mora-Flòrez, J. Meléndez, and G. Carrillo-Caicedo, "Comparison of impedance based fault location methods for power distribution systems," *Electr. Power Syst. Res.*, vol. 78, no. 4, pp. 657–666, 2008.

[6] M. Mirzaei, M. Z. A. A. Kadir, E. Moazami, and H. Hizam, "Review of fault location methods for distribution power system," *Australian J. Basic Appl. Sci.*, vol. 3, no. 3, pp. 2670–2676, 2009.

[7] R. Živanović, "Evaluation of transmission line fault-locating techniques using variance-based sensitivity measures," in *Proc. 16th Power Syst. Comput. Conf.*, Jul. 2008, pp. 1–6.

[8] M. M. I. Hashim, H. W. Ping, and V. K. Ramachandaramurthy, "Impedance-based fault location techniques for transmission lines," in *Proc. IEEE Region TENCON*, Jan. 2009, pp. 1–6.

[9] A. L. Dalcastagnê and S. L. Zimath, "A study about the sources of error of impedance-based fault location methods," in *Proc. IEEE/PES Transmission Distrib. Conf. Expo., Latin America*, Aug. 2008, pp. 1–6.

[10] E. O. Schweitzer, III, "A review of impedance-based fault locating experience," in *Proc. 14th Annu. Iowa-Nebraska Syst. Protect. Seminar*, Oct. 1990.

[11] K. Zimmerman and D. Costello, "Impedance-based fault location experience," in *Proc. 58th Annu. Conf. Protect. Relay Eng.*, Apr. 2005, pp. 211–226.

[12] V. Núñez, S. Kulkarni, S. Santoso, and M. Joaquim, "Feature analysis and classification methodology for overhead distribution fault events," in *Proc. IEEE Power Energy Soc. General Meeting*, Jul. 2010, pp. 1–8.

[13] M. M. Saha, J. J. Izykowski, and E. Rosolowski, *Fault Location on Power Networks*, 1st ed. New York, NY, USA: Springer-Verlag, 2010.

[14] T. Takagi, Y. Yamakoshi, M. Yamaura, R. Kondow, and T. Matsushima, "Development of a new type fault locator using the one-terminal voltage and current data," *IEEE Trans. Power App. Syst.*, vol. PAS-101, no. 8, pp. 2892–2898, Aug. 1982.

[15] L. Eriksson, M. M. Saha, and G. D. Rockefeller, "An accurate fault locator with compensation for apparent reactance in the fault resistance resulting from remote-end infeed," *IEEE Trans. Power App. Syst.*, vol. PAS-104, no. 2, pp. 423–436, Feb. 1985.

[16] *Transmission Line Protection Support Tools: Fault Location Algorithms and the Potential of Using Intelligent Electronic Device Data for Protection Applications*, EPRI, Palo Alto, CA, USA, Tech. Rep. 3002002381, 2013.

[17] D. Novosel, D. Hart, Y. Hu, and J. Myllymaki, "System for locating faults and estimating fault resistance in distribution networks with tapped loads," U.S. Patent 5 839 093, Nov. 17, 1998.

[18] A. Amberg, A. Rangel, and G. Smelich, "Validating transmission line impedances using known event data," in *Proc. 65th Annu. Conf. Protect. Relay Eng.*, Apr. 2012, pp. 269–280.

[19] E. O. Schweitzer, III, "Evaluation and development of transmission line fault-locating techniques which use sinusoidal steady-state information," *Comput. Elect. Eng.*, vol. 10, no. 4, pp. 269–278, 1983.

[20] D. A. Tziouvaras, J. B. Roberts, and G. Benmouyal, "New multi-ended fault location design for two- or three-terminal lines," in *Proc. IEE 7th Int. Conf. Develop. Power Syst. Protect.*, Apr. 2001, pp. 395–398.

[21] *Applications of PSCAD/EMTDC*, Manitoba HVDC Research Center Inc., Winnipeg, MB, Canada.

[22] W. H. Kersting, *Distribution System Modeling and Analysis*, 3rd ed. Boca Raton, FL, USA: CRC Press, 2012.

[23] T. A. Short, *Electric Power Distribution Handbook*. Boca Raton, FL, USA: CRC Press, 2004.

[24] R. E. Fehr. (2004, May). Sequence impedances of transmission lines [Online]. pp. 1–6. Available: http://helios.acomp.usf.edu/~fehr/carson.pdf

[25] H. Markiewicz and A. Klajn, "Earthing systems-fundamentals of calculation and design," in *Power Quality Application Guide*. Hertfordshire, U.K.: Copper Development Association, 2003.

[26] A. Apostolov, D. Tholomier, S. Sambasivan, and S. Richards, "Protection of double circuit transmission lines," in *Proc. 60th Annu. Conf. Protect. Relay Eng.*, Mar. 2007, pp. 85–101.

SWAGATA DAS received the B.Tech. degree from SRM University, Chennai, India, in 2009, and the M.S.E. degree from The University of Texas at Austin, Austin, TX, USA, in 2011, both in electrical engineering, where she is currently pursuing the Ph.D. degree in electrical engineering. She has interned with Development Consultants Pvt. Ltd., Kolkata, India, Hubbell Power Systems, Leeds, AL, USA, and Baker Hughes, Houston, TX, USA. Her research interests are fault location, power quality, and smart grid technologies.

SURYA SANTOSO (M'96–SM'02) received the B.S. degree from Satya Wacana Christian University, Salatiga, Indonesia, in 1992, and the M.S.E. and Ph.D. degrees in electrical engineering from The University of Texas at Austin, Austin, TX, USA, in 1994 and 1996, respectively. From 1997 to 2003, he was a Consulting Engineer with Electrotek Concepts, Knoxville, TN, USA. He is currently an Associate Professor with the Department of Electrical and Computer Engineering, The University of Texas at Austin. His research interests include power quality, power systems, and wind power.

ANISH GAIKWAD (M'00) is a Project Manager with the Grid Operations and Planning Group, Electric Power Research Institute (EPRI), Knoxville, TN, USA. His current activities focus on EPRIs research projects related to transmission planning. He is leading EPRIs research efforts on developing advanced planning tools for transmission network analysis and risk-based planning. His main areas of interest are modeling and model validation for transmission planning studies, risk-based transmission planning, interconnection studies, transient studies, and insulation coordination. He is involved in the distribution studies related to conservation voltage reduction, improving distribution efficiency, and modeling and analysis related to distribution systems.

MAHENDRA PATEL (M'74–SM'81) is a Technical Executive with the Grid Operations and Planning Department, Electric Power Research Institute (EPRI), Knoxville, TN, USA. He is involved in the research of synchrophasor technology, system protection, renewable integration, and advance grid monitoring and control applications. Before joining EPRI, he worked at PJM, participating in the evaluation, development and deployment of advanced technologies and processes for various PJM divisions. He has more than 40 years of experience in the Electric Power Industry in transmission planning and system reliability, transmission technologies, system dynamics, synchrophasor technology, switching surges and insulation coordination, voltage stability, system protection and power quality. He received the B.E. in electrical engineering from Sardar Patel University, Vallabh Vidyanagar, India, the M.S.E.E. degree from West Virginia University, Morgantown, WV, USA, and M.B.A. degree from the University of Pittsburgh, Pittsburgh, PA, USA.

● ● ●